iScience

CellPress
OPEN ACCESS

Article

Early cellular and molecular signatures correlate with severity of West Nile virus infection

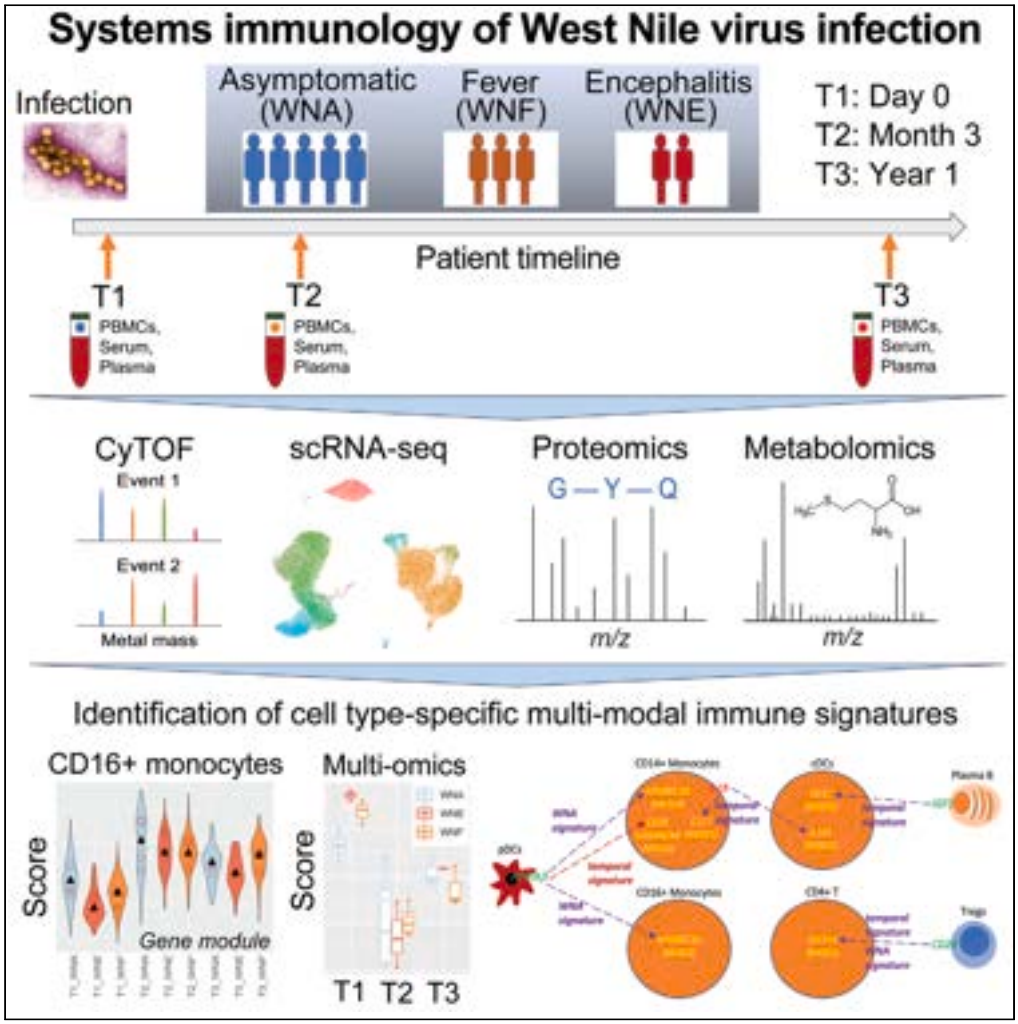

Ho-Joon Lee, Yujiao Zhao, Ira Fleming, ..., Kristy O. Murray, Steven H. Kleinstein, Ruth R. Montgomery

ruth.montgomery@yale.edu

Highlights

Systems immunology of peripheral blood from patients infected with West Nile virus

Longitudinal multi-omics profiling of asymptomatic and symptomatic patients

Differential immune states of Treg cells and CD16^{+} monocytes at acute time points

Identification of molecular signatures for infection severity and host cellular activity

Lee et al., iScience *26*, 108387
December 15, 2023 © 2023 The Author(s).
https://doi.org/10.1016/j.isci.2023.108387

iScience

CellPress
OPEN ACCESS

Article

Early cellular and molecular signatures correlate with severity of West Nile virus infection

Ho-Joon Lee,[1,15] Yujiao Zhao,[2,15] Ira Fleming,[3,4,5,15] Sameet Mehta,[1] Xiaomei Wang,[2] Brent Vander Wyk,[2] Shannon E. Ronca,[6] Heather Kang,[4] Chih-Hung Chou,[4] Benoit Fatou,[7] Kinga K. Smolen,[7] Ofer Levy,[8] Clary B. Clish,[4] Ramnik J. Xavier,[4,9,10] Hanno Steen,[6] David A. Hafler,[11] J. Christopher Love,[3,4,5] Alex K. Shalek,[3,4,5] Leying Guan,[12] Kristy O. Murray,[6] Steven H. Kleinstein,[13,14] and Ruth R. Montgomery[2,16,*]

SUMMARY

Infection with West Nile virus (WNV) drives a wide range of responses, from asymptomatic to flu-like symptoms/fever or severe cases of encephalitis and death. To identify cellular and molecular signatures distinguishing WNV severity, we employed systems profiling of peripheral blood from asymptomatic and severely ill individuals infected with WNV. We interrogated immune responses longitudinally from acute infection through convalescence employing single-cell protein and transcriptional profiling complemented with matched serum proteomics and metabolomics as well as multi-omics analysis. At the acute time point, we detected both elevation of pro-inflammatory markers in innate immune cell types and reduction of regulatory T cell activity in participants with severe infection, whereas asymptomatic donors had higher expression of genes associated with anti-inflammatory CD16^{+} monocytes. Therefore, we demonstrated the potential of systems immunology using multiple cell-type and cell-state-specific analyses to identify correlates of infection severity and host cellular activity contributing to an effective anti-viral response.

INTRODUCTION

West Nile virus (WNV) is a global mosquito-borne pathogen which can cause severe neurological illness, especially in immunocompromised and older individuals.[1,2] Since being introduced to the United States in 1999, the virus has spread through North and South America[3] and more than 51,000 cases have been reported, including 2,390 fatalities.[4,5] By 2016, infections in the USA were estimated at 7 million people.[6] While about 80% of infected people have an asymptomatic infection, approximately 20% experience mild illness with fever symptoms, and a minority of cases (~1%) experience severe, neuroinvasive disease.[7]

To understand the broad range of clinical symptoms and determinants of susceptibility to severe WNV disease, we must consider elements of the pathogen, vector, and host. The dominant circulating strain of WNV in North America since 2001 (WN2002) and the proportion of severe cases reported across the country have remained fairly constant over two decades.[3–5] Thus even though environmental variation in climate, mosquito, and bird populations are relevant for the frequency of exposures,[8] variations in host responses contribute significantly to the range of disease severity in human cases.

[1]Department of Genetics and Yale Center for Genome Analysis, Yale School of Medicine, New Haven, CT 06520, USA
[2]Department of Internal Medicine, Yale School of Medicine, New Haven, CT 06520, USA
[3]The Institute of Medical Science and Engineering, Department of Chemistry, and Koch Institute for Integrative Cancer Research, MIT, Cambridge, MA 02139, USA
[4]Broad Institute of MIT and Harvard, Cambridge, MA 02142, USA
[5]The Ragon Institute of MGH, MIT, and Harvard, Cambridge, MA 02139, USA
[6]Department of Pediatrics, National School of Tropical Medicine, Baylor College of Medicine and Texas Children's Hospital, Houston, TX 77030, USA
[7]Department of Pathology, Boston Children's Hospital and Harvard Medical School, Boston, MA 02115, USA
[8]Department of Infectious Disease, Precision Vaccines Program, Boston Children's Hospital, and Harvard Medical School, Boston, MA 02115, USA
[9]Center for Computational and Integrative Biology and Department of Molecular Biology, Massachusetts General Hospital and Harvard Medical School, Boston, MA 02114, USA
[10]Klarman Cell Observatory, Broad Institute of MIT and Harvard, Cambridge, MA 02142, USA
[11]Departments of Neurology and Immunobiology, Yale School of Medicine, New Haven, CT 06510, USA
[12]Department of Biostatistics, Yale School of Public Health, New Haven, CT 06520, USA
[13]Department of Pathology, Yale School of Medicine, New Haven, CT 06520, USA
[14]Program in Computational Biology and Bioinformatics, Yale University, New Haven, CT 06520, USA
[15]These authors contributed equally
[16]Lead contact
*Correspondence: ruth.montgomery@yale.edu
https://doi.org/10.1016/j.isci.2023.108387

This is an open access article under the CC BY-NC-ND license (http://creativecommons.org/licenses/by-nc-nd/4.0/).

Table 1. Demographics of study participants

Parameter	Asymptomatic (n = 4)	Symptomatic (n = 7)	Total (n = 11)	p value
Mean age (yr) (SD)	67.8 (7.4)	52.9 (14.0)	58.3 (13.9)	0.0471[a]
range	59–77	28–68	28–77	
No. (%) of females	0 (0)	2 (29)	2 (18)	0.0215[b]

[a]Age: Using t test, two-tailed.
[b]Gender: Using Chi-square test.

A number of host factors are relevant for susceptibility to severe WNV. These include genetic analyses that identified variations in several immune-related genes in individuals at increased risk for severe disease[9–11] including those involved in type I interferon (IFN) pathways which are critical for control of WNV infection.[12] The critical role of type I IFN pathway has been confirmed in experimental studies[13,14] as have immune pathways involved in recognition and clearance of WNV, including RIG-I mediated immune responses.[1,7,15–17] Moreover, recent studies of multiple cohorts of WNV disease from the EU and the USA showed that auto-antibodies neutralizing IFN-α and/or IFN-ω are found with greater frequency in patients with severe infection and accounted for at least a third of 441 hospitalizations for life-threatening WNV disease.[18,19] Notably, age is a critical risk factor for WNV, and the majority of severe cases are over age 60.[5,8] Aging is associated with a well-documented decline in immune recognition and signaling by pathogen recognition receptors such as Toll-like receptors (TLRs), RIG-I (retinoic acid-inducible gene I), and RLR (RIG-like receptors), highly relevant for responses to infection with WNV and type I IFN responses to viral infections such as WNV and influenza and responses to vaccination.[20–25] But while symptomatic WNV infection occurs predominantly in older people,[26] there is no significant difference with age among asymptomatic participants, underscoring the critical role of individual host response mechanisms.[27]

Investigating transcriptional and functional immune responses in blood of recovered WNV patients, we previously identified a susceptibility signature in innate immune cells including interferon pathways, production of the chemokine CXCL10, and a key role for reduced induction of pro-inflammatory cytokine interleukin (IL)-1β in severe infection.[28] IL-1β has also been shown to be critically important for control of WNV in the brain.[29] In addition, symptomatic patients have been reported with reduced numbers of T cell subsets (Th1/Th17 and Tregs) and elevated expression of Tim-3$^+$ and atypical T cells.[30–32] Notably, antibodies against WNV were durable and were not different between asymptomatic and symptomatic adults for titer or epitopes targeted.[33] However, studying samples collected after infection resolves, we cannot distinguish whether features may be a cause or a consequence of clinical severity. Taking advantage of advances in systems immunology, and an unusual recruitment strategy, we investigated immune responses during acute infection from asymptomatic and symptomatic participants using multiple omics profiling platforms and integrating high resolution methods of cellular, transcriptomic, proteomic, and metabolomic analyses. Comparing stratified participants longitudinally at acute and convalescent time points, we have taken advantage of stable characteristics of immune cell frequencies and gene expression in individuals[34–36] to identify molecular signatures and cell states and integrated temporal responses associated with resistance to severe WNV infection. These signatures may provide relevant guidance for timely therapeutic responses in severe infections.

RESULTS

WNV study population for longitudinal immunophenotyping profiles

To investigate immune-related differences in infection with WNV contributing to the divergence in the clinical course and identify responses related to severe infection, we enrolled two groups of WNV participants in Houston, TX. Hospitalized patients had acute CDC-defined WNV infection including clinical criteria of mild symptomatic response or severe neurologic disease, with no specific treatments for WNV.[37] We enrolled acutely infected asymptomatic participants found to be viremic while volunteering to donate blood. Our unusual recruitment criteria allowed us to enroll both severity groups at comparable duration of viral exposure (~7 days). Immune signatures from asymptomatic (WNA) and symptomatic (WNF fever and WNE neurologic) study participants were assessed at enrollment (Day 1) and at follow-up time points of Month 3 and Year 1 of convalescence (n = 11; Table 1).

Immune cell frequency and functional status in WNV infection

For profiling frequency and functional status of immune cells, we assessed whole blood samples using the SMART Tube system to stabilize cell phenotypes.[38] Untreated cryopreserved samples were profiled using CyTOF, employing a 40-marker antibody panel to broadly quantify both immune cell lineages and functional markers (Table S1). To reduce experimental variation, all samples were assayed together using a uniform lot of reagents and including a spike-in reference with each sample as described previously.[39] Data from the reference cells partitioned from WNV samples were assessed by PCA. No evidence of batch effect from the reference cells was observed across all symptom status or time points of sample collection (Figure S1).

Cell types from whole blood samples were manually annotated based on characteristic lineage markers (Figure 1A) using a defined cell ontology (Figure S2B).[40] Using a whole blood sample allows a detailed examination of 29 cell subsets including polymorphonuclear leukocytes (PMN), the most abundant immune cell type in circulation, and 28 subsets of peripheral blood mononuclear cells (PBMCs). Many infection-related differences in cell frequency were detected in both asymptomatic and symptomatic groups. Analysis of cell frequencies for each individual showed an elevated frequency of PMN in total cells at acute viral infection compared with his/her own convalescent sample at Month 3 time point

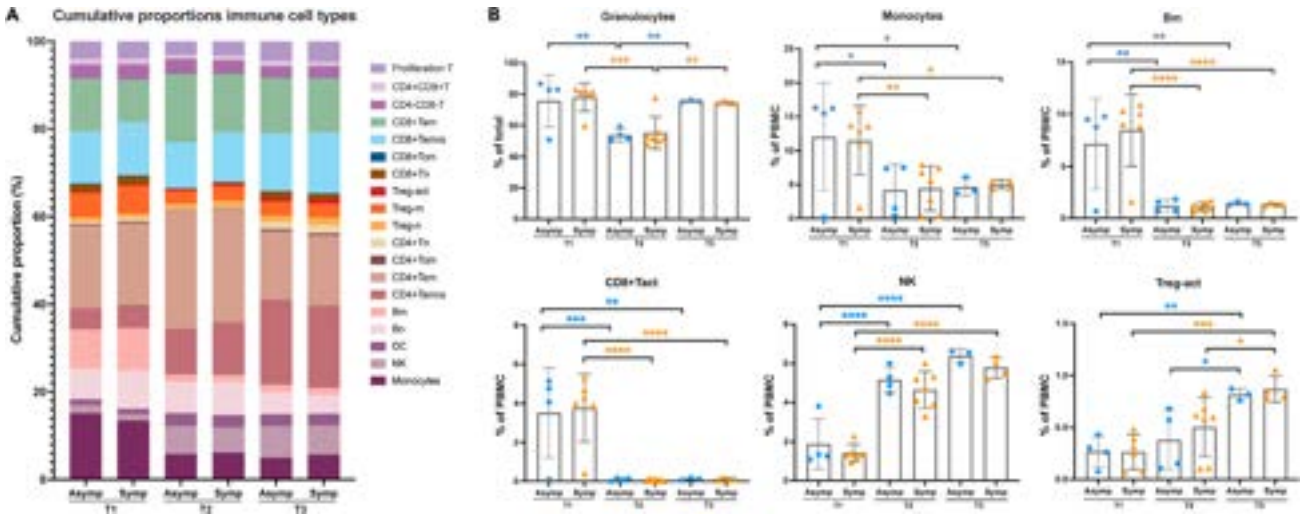

Figure 1. Frequency of immune cell subsets of WNV infected participants

Blood samples were collected into SMART tubes from WNV asymptomatic (n = 4) and symptomatic (n = 7) participants at acute Day 1 and convalescent time points at Month 3 and Year 1. Whole blood cells were labeled for immune cell markers and profiled by CyTOF in one batch. Frequency of PMN and 28 PBMC subsets were defined by expression of lineage markers (Figure S2B).

(A) Frequency of 28 PBMC subsets shows the variation of cell frequencies in asymptomatic and symptomatic groups at the time points indicated for cell types shown ($CD4^+$ and $CD8^+$ subsets for naive (n), effector memory (em), central memory (CM), activated (act), and effector (Temra).

(B) Differences in frequencies of cell subsets between cohorts and time points were assessed by one-way ANOVA with Tukey's multiple comparisons test (*$p < 0.05$, **$p < 0.01$, ***$p < 0.001$, and ***$p < 0.0001$). No significant frequency differences were found between asymptomatic and symptomatic groups. Data are represented as mean ± SD. See also Figures S1 and S2.

(Figure 1B; Day 1 vs. Month 3 $p = 0.003$ for asymptomatic; $p = 0.0002$ for symptomatic). No significant differences for frequency of PMN were noted between severity groups (Figure 1B). We have previously shown a biphasic role for PMN in murine WNV infection with an initial phase permissive for viral replication and contributing to dissemination and subsequently later in infection controlling viremia.[41] Within PBMCs other innate immune cell types also showed significant elevations at the acute time point reflecting expected increases during an acute viral infection.[39,42] Levels of $CD14^+$ classical monocytes in PBMCs were elevated at Day 1 for all participants compared to each individual's Month 3 and Year 1 of convalescence (Figure 1B; acute vs. Month 3 $p = 0.0199$ for asymptomatic; $p = 0.009$ for symptomatic). Overall, we detected elevated frequencies >1.1-fold for 18 of 28 PBMC cell subsets during acute infection compared to convalescent time points, including a marked elevation in the frequency of memory B cells (Bm), which may be expected as antibody responses develop (Figure 1B; Day 1 vs. Month 3 $p = 0.0015$ for asymptomatic; $p < 0.0001$ for symptomatic). All subject groups showed elevated levels of activated $CD8^+$ T cells ($CD8^+$ T) at Day 1 compared to convalescent time points (Figure 1B; Day 1 vs. Month 3 $p = 0.0013$ and 0.0005 for asymptomatic; $p < 0.0001$ for symptomatic). A similar pattern was noted in activated $CD4^+$ T cells (Day 1 vs. Month 3 $p = 0.0013$ for asymptomatic; $p < 0.0001$ for symptomatic).

While many cell types were more abundant during acute infection, in contrast, we detected significantly lower frequencies at Day 1 for natural killer (NK) cells (Figure 1B; $p < 0.0001$ for asymptomatic; $p = 0.0002$ for symptomatic). We previously showed that a more immature subset of NK cells is highly responsive to WNV with degranulation and cytokine production.[43] Significant increases over the time course were also detected for levels of activated Tregs (Treg-act) which have an important role in resolution of inflammation (Figure 1B; Day 1 vs. Year 1 $p = 0.0028$ for asymptomatic; $p = 0.0002$ for symptomatic). These increased levels over time are consistent with previous reports for symptomatic WNV patients[30] and notably were equivalent between asymptomatic and symptomatic participants. Overall, quantifying frequencies of multiple immune lineages showed consistent changes longitudinally in cell type abundance whether or not participants experienced symptomatic illness. This reveals ongoing "shadow" immune responses in asymptomatic individuals and suggests that cell frequency alone is not sufficient to distinguish immune responses leading to severe disease.

In our phenotyping profile, we quantified 20 markers of cellular activation to assess functional changes which may contribute to susceptibility to severe infection. This multiparameter platform allows us to interrogate each marker in 29 cell subsets for a total of 580 marker/cell type combinations. In response to infection with WNV, we detected elevated proinflammatory activity in multiple cell types at the acute time point with levels decreasing at Month 3 and Year 1 (Figure 2A; Figures S3A and S3B). Remarkably, numerous activation markers were altered equivalently across subject severity cohorts with 451/580 combinations being higher at Day 1 compared to Month 3. Highly expressed markers at the acute time point included L-selectin adhesion molecule CD62L, marker of activation of PMN and monocytes, and an important factor for lymphocyte trafficking out of the blood.[44] Elevated levels of CD41, the integrin glycoprotein IIb/IIIa, were also detected in multiple cell lineages during acute infection, which may reflect interactions with platelets which are readily apparent in the whole blood samples being examined here. This finding is consistent with well-characterized binding of platelets to activated leukocytes.[45] In addition, CD41 was expressed on precursor cells which may be more abundant during acute infection.[46] The marker CD279 (PD-1) was elevated at the acute compared to

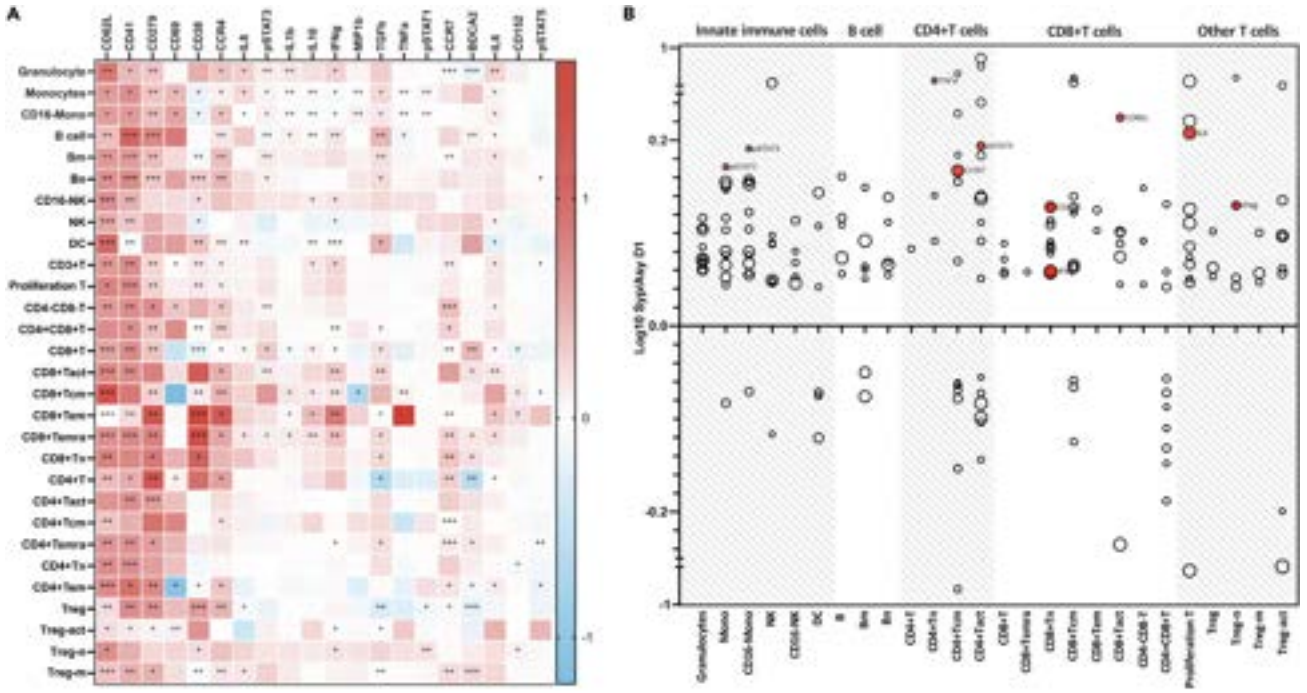

Figure 2. Altered immune functional markers during acute WNV infection

Whole blood cells from WNV patients (n = 11) were labeled with metal-conjugated antibodies and analyzed by mass cytometry to quantify levels of 20 functional markers in 28 cell subsets.

(A) Change in median channel intensity at acute vs. Month 3 convalescent time point (ratio log10 acute/convalescent). Significance by generalized linear mixed model with *p < 0.05, **p < 0.01 and ***p < 0.001.

(B) Log10 ratio of symptomatic/asymptomatic of marker/cell type combinations shown for individual cell subsets with fold change of greater than 10% of baseline where size of circle reflects the average expression level of a marker in a cell type. Statistically significant combinations in permutation analysis are shaded in red, where the observed log ratio of expression in symptomatic relative to asymptomatic occurred less than 5% of the time in the permuted distribution. See also Figures S1–S3.

Month 3 time point, which may be important for development of $CD8^+$ T cell memory responses.[47] These elevations in immunomodulatory markers resolved and were not significant between groups at Month 3 or Year 1 (Figure S3).

To investigate functional differences contributing to the divergence in the clinical course, we identified marker/cell type combinations that were significantly different between symptomatic and asymptomatic participants. Of the 274 cell type/marker combinations above a threshold of 20% of baseline of mean channel intensity, we found 181 cell type/marker combinations expressing intensity differences >10% between severity groups (Figure 2B). At the acute time point in symptomatic participants, we detected significant elevations for combinations of pro-inflammatory functional markers in innate immune cell types, including elevated expression of cytokines (IL-1β, MIP1β, IL-6, IL-8, and TNFα) in PMN and in monocytes; phosphorylated signaling intermediates (pSTAT1 and pSTAT3) and the inflammatory marker CD62L, known as L-selectin, in PMN, monocytes, NK, and DC (Figure 2B, p = 0.038 and 0.024 for pSTAT3 in monocytes and $CD16^-$ monocytes). Elevations in functional markers in adaptive cell types in symptomatic participants include TNFα in naive CD4+T cells (p = 0.049), CCR7 in $CD4^+$ T cells (p = 0.006), pSTAT5 in activated $CD4^+$ T cells (p = 0.012), and numerous markers in $CD8^+$ T cells including CD62L, CD152, and IFNγ and CD69, the C-lectin receptor marker of lymphocyte activation increased in several subsets of T cells ($CD4^+$ Tem, $CD4^+$Tact cells, and naive Treg) (Figure 2B, p = 0.042/0.034 for IFNγ/CD152 in naive $CD8^+$ T cells; p = 0.022 for CD62L in activated $CD8^+$ T cells). The elevated expression in symptomatic patients of phospho STAT3 in monocytes and phospho STAT5 in $CD4^+$ T cells identifies key pathways increasing production of inflammatory cytokines such as IL-6. An elevated inflammatory milieu has previously been reported to contribute to permeability of the blood-brain barrier,[48] thus the skewing toward pro-inflammatory responses in symptomatic participants may contribute to severity of infection. A lower inflammatory profile in asymptomatic participants may be beneficial for antiviral responses. Comparing longitudinally for each individual, no significant differences were detected between asymptomatic and symptomatic participants at convalescent time points suggesting that key differences in clinical trajectory occur during acute infection.

Transcriptional profiles of immune response to WNV infection

To collect additional in-depth measurements of cellular function during WNV infection and investigate functional differences contributing to the divergence in clinical course, we assessed transcriptional profiles as an additional measure of functional status to track changes in cell responses during infection with WNV. We used PBMCs collected at the same time points from our study participants to identify differential

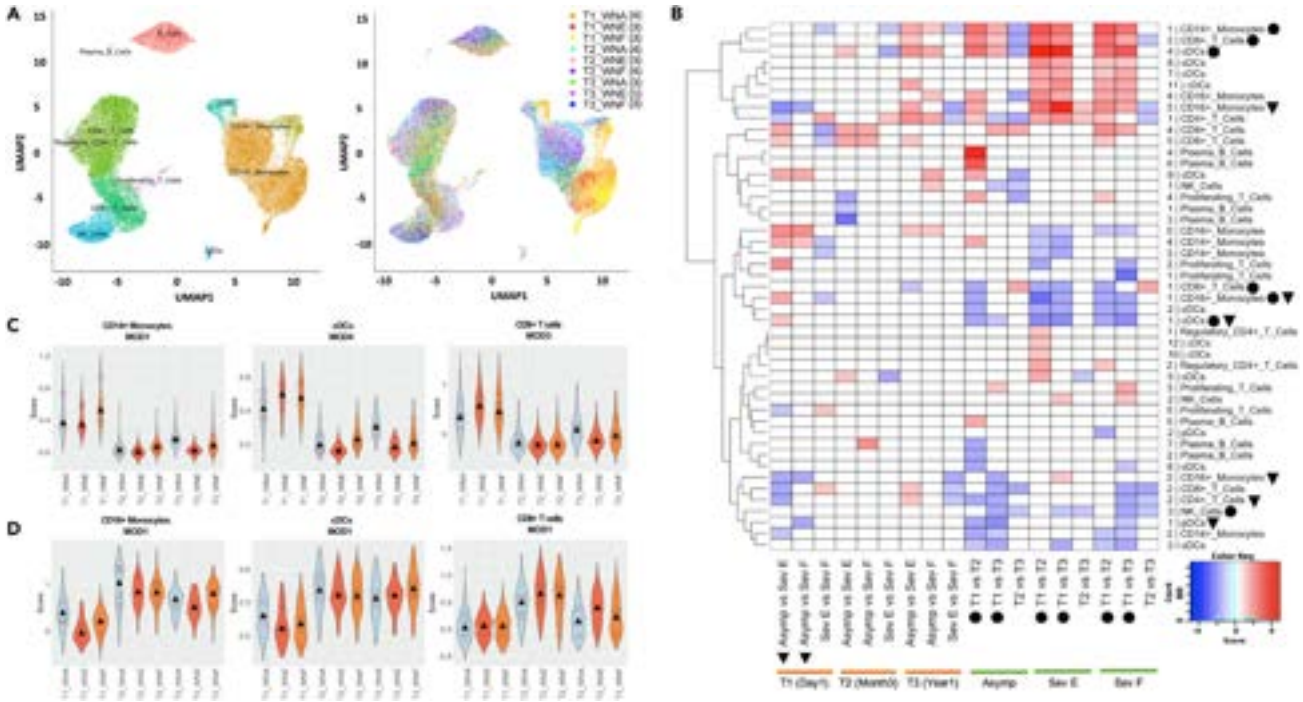

Figure 3. Seq-Well transcriptomic analysis of response to WNV infection

(A) UMAP projection shows distribution of 11 cell types and 9 cell states. WNA = Asymptomatic, WNE = encephalitis, WNF = fever, T1 = Day 1, T2 = Month 3, and T3 = Year 1 with the number of participants in parentheses for each respective condition.

(B) Heatmap of signed module scores for 42 differential modules and 18 condition pairs for which there are significant differences with fold change >1.3 and mean p value <0.01. For a given condition pair in each column, positive (red) and negative (blue) reflect a higher module score in the first condition score or second condition, respectively. Condition pairs are marked for significant differences between time points (circle; ●) and between severity groups (triangle; ▼).

(C) Violin plots of module scores for 3 differential modules of interest elevated at the T1 time point. The subject-level median values in each condition are shown in open circles, while the condition-level median values in solid triangles.

(D) Violin plots as in (C) decreased at the T1 time point. See also Figure S4, Data S2, and Tables S2 and S3.

expression patterns longitudinally and relevant to severe infection. PBMCs were assessed using the Seq-Well platform for efficient single-cell RNA-seq.[49] PBMC samples provided 5,243 transcripts and 1,776 genes per cell on average for 56,858 cells sequenced and pre-processed. Cell types were identified by unsupervised clustering and differential expression analysis together with 36 canonical lineage marker genes in an iterative manner using the Seurat R package (Figure 3A; Figure S4).[50] The uniform manifold approximation and projection (UMAP) displays 11 cell types with innate cell lineages (conventional and plasmacytoid dendritic cells (cDCs and pDCs), monocytes, natural killer, NK) separated from T cell subsets and B cells (Figure 3A). Notably, UMAP shows separation of the 3 severity groups by time points—acute (T1), Month 3 (T2), and Year 1 (T3)—where samples from the acute time point clustered together most closely and later time points show considerable mixing among severity groups indicating the transcriptional similarity of cells. As expected, the frequencies of cell types defined by gene expression are consistent with but not identical to cell frequencies defined in CyTOF by protein expression markers, showing slight differences between the two platforms.

Gene modules reveal transcriptional responses to WNV infection

Using expression data for the 11 cell types, we used the weighted gene co-expression network analysis (WGCNA)-based module discovery[51] to first identify *significant modules* of co-expressed genes for each of the 11 cell types. We compared all possible condition pairs to identify *differential modules* for the 18 condition pairs. There were 107 significant modules identified from 10 cell types (excluding B cells), from which we identified 47 *differential modules* with fold change >1.3 and mean p value <0.01 in at least one condition pair (Figure 3B; Table 2) with both elevated and reduced gene expression for all severity groups. The numbers of module genes range from 10 in module 2 of pDCs to 161 in module 1 of $CD14^+$ monocytes. We gave particular attention to 12 modules from eight cell types selected by visual assessment of module score distributions showing the most dramatic differences between time points or severity groups as well as the top 10 genes in each module whose expression profiles are most correlated with the module scores (Table S2). For temporal signatures, we identified module 1 in $CD14^+$ monocytes, module 1 in $CD16^+$ monocytes, modules 1 and 3 in $CD8^+$ T cells, modules 1 and 4 in cDCs, and module 3 in NK cells. For signatures reflecting disease severity, we identified modules 1, 2, and 3 in $CD16^+$ monocytes, module 2 in $CD4^+$ T cells, modules 1 and 4 in cDCs, module 1 in pDCs, and module 6 in plasma B cells. The majority of differential modules revealed signatures related to the time course of

Table 2. Top pathways in Seq-Well differential modules

Cell type	Module	Number of genes per module	Top pathways in module
CD14$^+$ Monocytes	1	162	HIF-1; hypoxia; glycolysis; IL-2/STAT5
CD16$^+$ Monocytes	1	16	Leishmaniasis; Yersinia infection; Apical Junction; mTORC1
CD16$^+$ Monocytes	2	11	Amphetamine addiction; IL-17; TNF-α/NF-kB
CD16$^+$ Monocytes	3	16	Mineral absorption; Iron metabolism; Apoptosis; IL-2/STAT5
CD4$^+$ T Cells	2	11	Osteoclast differentiation; TNF- α/NF-kB; Neuroinflammation
CD8$^+$ T Cells	1	35	Bacterial invasion of epithelial cells; Pathogenic Escherichia coli infection; Interferon Gamma Response
CD8$^+$ T Cells	3	20	NOD-like receptor signaling; Ferroptosis; TGF-β; TNF-α/NF-kB
cDCs	1	109	Hematopoietic cell lineage; Macrophage markers; Complement system of innate immunity
cDCs	4	119	Ferroptosis; HIF-1; NAD metabolism, sirtuins and aging; TNF-α/NF-kB; Inflammatory response
NK Cells	3	15	Neuroinflammation; TNF-α/NF-kB; hypoxia; TGF-β
pDCs	1	11	IL-17; Neuroinflammation; TGF- β; TNF-α/NF-kB; hypoxia
Plasma B Cells	6	32	N-Glycan biosynthesis; Interferon gamma response; IL-2/STAT5; TNF-α/NF-kB

In-depth analysis for 12 selected differential modules identified using Weighted Gene Co-Expression Network Analysis (WGCNA) framework. Top pathways were identified using Enrichr.

infection, with significant changes from the acute time point Day 1 (T1) to the convalescent time point at Month 3 (T2) or Year 1 (T3). For example, the module scores and marker expression were higher in T1 than T2 and T3 in all severity groups for module 1 in CD14$^+$ monocytes, for module 4 in cDCs, and for module 3 in CD8$^+$ T cells (Figure 3C).

Examination of the upregulated genes in these modules revealed many genes relevant for response to acute viral infection and innate immune pathways. In particular, module 1 in CD14$^+$ monocytes, which is upregulated in acute infection, contained 162 genes which are enriched in critical pathways to support cell metabolic function and to initiate immune cell responses (hypoxia and glycolysis, HIF-1, and IL-2 signaling). The top differentially expressed genes in CD14$^+$ monocyte module 1 include genes involved in cell attachment and integrin signaling reflecting the need for dynamic rearrangements of the actin cytoskeleton for spatial reorganization of receptors and adhesion molecules: *TIMP1*, a metalloproteinase inhibitor which plays a role in integrin signaling and activates cellular signaling cascades via CD63 and ITGB1; *SDC2*, a heparan sulfate proteoglycan which has been implicated in regulation of cytoskeleton organization and integrin signaling; *THBS1*, thrombospondin, an adhesive glycoprotein that mediates cell-to-cell and cell-to-matrix interactions; and *SERPINB2*, a regulator of cell movement.[52] Detailed examination of genes highly expressed in CD14$^+$ monocytes module 1 at the acute time point includes (a) *CD86*, a marker of activated dendritic cells; (b) cytokines, chemokines and their receptors (*ILIRN*, *CCL2*, *IRF1*, *IL6R*, *CLEC5A*, *CCL7*, *IFITM10*, *CD9*, *CSF1*, *DOCK4*, *ILIR1*); (c) signaling elements including *MAP3K8*, *NFkB1*, and *HIPK2* which we have shown is necessary for interferon response in WNV infection by phosphorylating the transcription factor *ELF4*[53]; and (d) *DUSP4* and *DUSP5*, dual tyrosine/threonine phosphatases which regulate immune cell activity by inactivating MAP kinases.[54] The 162 genes in CD14$^+$ monocyte module 1 reflect key responses needed to mount an immune response to viral infection. Notably, the number of monocytes was highly elevated in frequency at the acute time point (Figure 1B) thus further amplifying the net levels of these genes in acute infection.

Module 4 for cDCs, also enriched at the acute time point, includes immune signaling genes related to HIF-1, inflammatory response, and TNFα/NFκβ pathways. Many of the innate immune response genes in this module are shared with CD14$^+$ monocytes module 1–36 genes in common—such as *CD86*, SERPIN family genes, *TIMP1*, *SDC2*, *JARID2*, *DUSP4*, and chemokine and TNF pathway genes (Table S3). In addition to the responses from innate immune cell types, genes in module 3 from CD8$^+$ T cells were highly expressed at the acute time point and enriched in pathways for TNFα/NFκβ as well as NOD signaling pathways. Top genes expressed in this module also include genes involved in transcriptional regulation and signaling, e.g., JMJD1C (KDM3C) histone H3K9 demethylase, *PMEPA1*, a negative regulator of TGF-β signaling,[55] and *LUZP1*

(leucine zipper protein 1), an actin-stabilizing protein[56] (Table S3). The increased average expression of $CD8^+$ T cell module 3 genes correlates with the elevated frequency of $CD8^+$ T cells identified by CyTOF at this time point across severity groups, consistent with a robust anti-viral response mounted by expanded $CD8^+$ T cells.

Concomitantly with the elevated modules were gene modules with lower expression at the acute time point, genes which may be down-regulated to enhance an effective anti-viral response (Figure 3D). Across severity groups at T1, we detected lower expression of module 1 of $CD16^+$ monocytes characterized by mTORC1 pathway; module 1 of cDCs defining pathways of hematopoietic cells and complement; and module 1 of $CD8^+$ T cells including genes in the IFNγ response (Table S3). Module 1 of $CD16^+$ monocytes includes the anti-viral protein *SAMHD1*, actin and actin binding protein *CAP1* and *LCP1* (L-plastin) that stabilizes integrin binding for the immune synapse with cytotoxic T cells,[57] and inflammatory mediator *CYBB*, cytochrome *b*-245 beta chain), a component of the phagocyte NADPH oxidase complex (Table S3). Three of the top 10 genes in cDC module 1 are members of the S100 family and have significant roles in immune signaling and responses. *S100A8* and *S100A9* are the subunits of the calcium- and zinc-binding heterodimer calprotectin, which is a biomarker of inflammation and a potent chemotactic factor[58] (Table S3). S100A4 is a calcium binding hypoxia-inducible gene (Table S3). Reduced expression of these genes reflects the regulated program of cellular responses to viral infection and for these genes was not found to be different between asymptomatic and symptomatic cases.

Gene modules distinguish WNV severity groups

In addition to longitudinal changes in gene expression, our analysis detected modules which distinguish severity groups. The module scores were lower in asymptomatic compared to symptomatic groups for modules 2 and 3 in non-classical ($CD16^+CD14^-$/dim) monocytes, module 2 in $CD4^+$ T cells, and module 1 in pDCs. Asymptomatic participants had higher expression of module 1 in $CD16^+$ monocytes and module 1 for cDCs (Figure 3B). These gene changes identified in asymptomatic participants may be critical elements of immune responses relevant to reduced susceptibility to severe disease. Notably 4 of the 6 modules which distinguish severity groups were expressed at lower levels in asymptomatic donors suggesting either control of exuberant response to the virus may be a key part of asymptomatic infection or higher inflammatory responses occurred with symptomatic infection. Of the six modules showing the highest significant differences between severity groups, five modules are related to responses of innate cell types. In particular, $CD16^+$ monocytes, considered anti-inflammatory in some settings,[59] are the most highly represented (3 of 6 modules). Of particular interest is higher expression of genes at the acute time point by asymptomatic donors in $CD16^+$ monocytes module 1 (also shown to be lower at acute time point in all groups) which includes anti-viral protein *SAMHD1*, actin and actin binding protein *LCP1* and *CAP1* as detailed previously (Table S3). Module 1 in cDCs is higher in asymptomatic donors, including *CD62L* (SELL) previously noted to be elevated in CyTOF assays (Figure 2A); 5 genes in the S100 immune signaling family; and genes predominantly included in the type I IFN response such as *OAS3*.

Furthermore, asymptomatic donors at the acute time point show reduced expression of genes in modules 2 and 3 of $CD16^+$ monocytes compared to the severe patients with encephalitis. These modules include immune signaling intermediates *FOS*, *FOSB*, and *JUN*, in the TNFα signaling pathway, and genes related to apoptosis. Another top gene expressed by $CD16^+$ monocytes in module 3 is anti-inflammatory *ANAX1* (annexin A1).[60] Asymptomatic donors also show reduced expression of inflammatory genes in module 2 by $CD4^+$ T cells which may contribute to less severe responses. Top genes in $CD4^+$ T cells module 2 include *CITED2*, a transactivator which negatively regulates HIF-1, and transcription factors such as *RXRα*, *NF-κB*, *STAT2*[61] as well as other transcriptional regulators including *JUN*, *JUNB*, *NUNB*, *FOS*, *FOSB*, *SOCS3*. The collective differences between asymptomatic and symptomatic responses revealed here through the transcriptional analysis reflect reduced expression of pro-inflammatory and apoptotic signaling genes in asymptomatic donors. The asymptomatic response is also characterized by increased expression of genes involved in cytokine responses IFNγ and TNFα/NFκB, IL-2/STAT5 signaling, and an increased expression of IFN anti-viral genes.

Ligand-target interactions in transcriptional responses

Having identified those differential modules of co-regulated genes associated with stage of infection or with disease severity, we employed a ligand-target inference tool, *NicheNet*,[62] to infer potentially functional ligand-target pairs for the 12 modules of interest and to discover critical genes which may mediate communication between immune cells in response to WNV (Table 3). The 12 modules show dramatic changes over time or with disease severity and we wanted to know which ligands and pathways could be driving those changes and targeting genes in those modules. With data at a population level, we identified a particularly prominent role for IL-1β from $CD14^+$ monocytes as the top ligand mediating interactions between multiple cells including an autocrine interaction from module 1 targeting CCL7 in $CD14^+$ monocytes; and paracrine interactions from $CD14^+$ monocytes to target IL1R1 in module 4 of cDCs as well as CD83 in module 2 of $CD16^+$ monocytes. A critical role for IL-1β has been noted previously in distinguishing severity of WNV infection[28] and in control of WNV in the brain.[29] This analysis also identified TNF expressed by $CD16^+$ monocytes as the top ligand for autocrine signaling to target CSF1R and AHR in modules 1 and 3, respectively. The top ligand produced by $CD8^+$ T cells, INFγ, was found to multiply target JUNB in both module 2 of $CD4^+$ T cells and in module 1 of pDCs as well as IRF8 in module 6 of plasma B cells, all of which are associated with disease severity.

Ligand-target interactions were also inferred in chains or inter-cellular cascades, i,e., NFκβ1 in module 3 of $CD8^+$ T cells, which is enriched in NFκβ signaling as mentioned previously, is a target of OSM (oncostatin M), the top ligand of $CD14^+$ monocytes. OSM is an interleukin-6 family cytokine[63,64] and module 1 of cDCs serves as a target of IL-15 from $CD16^+$ monocytes. OSM was reported to be elevated during acute human anaphylaxis together with S100A8/A9,[65] two of the top three genes in module 1 of cDCs. Thus, we identified potentially important interacting factors that are highly relevant to anti-viral responses.

Table 3. Top ligand-target pairs in cell-cell communication

Receiver cell type	Module	Target	Ligand	Sender cell type	Activity Score
$CD8^+$ T Cells	1	GZMA	HMGB2	Proliferating T Cells	0.00860
$CD14^+$ Monocytes	1	CCL7	IL1β	$CD14^+$ Monocytes	0.00860
cDCs	1	OSM	IL15	$CD16^+$ Monocytes	0.00748
cDCs	4	IL1R1	IL1β	$CD14^+$ Monocytes	0.00695
$CD16^+$ Monocytes	1	CSF1R	TNF	$CD16^+$ Monocytes	0.00686
Plasma B Cells	6	IRF8	IFNγ	$CD8^+$ T Cells	0.00683
NK Cells	3	GADD45B	IL18	cDCs	0.00644
$CD16^+$ Monocytes	2	CD83	IL1β	$CD14^+$ Monocytes	0.00620
$CD16^+$ Monocytes	3	AHR	TNF	$CD16^+$ Monocytes	0.00585
$CD4^+$ T Cells	2	JUNB	IFNγ	$CD8^+$ T Cells	0.00569
pDCs	1	JUNB	IFNγ	$CD8^+$ T Cells	0.00569
$CD8^+$ T Cells	3	NFKB1	OSM	$CD14^+$ Monocytes	0.00265

The top ligand-target pairs were inferred by NicheNet analysis with the highest activity score for the 12 differential modules in Table 2. Each top ligand shows the highest expression in the 'sender' cell type shown.

Circulating soluble factors show proteins and metabolites affected by infection with WNV

To investigate the systemic milieu of the cellular immune responses and to determine which circulating factors are relevant to severity of WNV infection, we quantified proteins and metabolites in the serum of our subject cohort. We employed the MStern blotting-based proteomics platform for non-depleting profiling of the serum proteome with all high-abundance proteins remaining in the sample.[66–70] We examined longitudinally collected samples to quantify differentially abundant proteins from acute infection through convalescence and to distinguish the severity groups of WNV patients (Table S4). When comparing participants across time points, we identified 30 significant proteins, grouped into specific clusters which showed distinct patterns of enrichment over the time course and severity of WNV infection (Figure 4 $p < 0.05$; one-way ANOVA). In particular, we identified several proteins associated with acute phase response and inflammatory processes including the complement and coagulation pathways.[71]

Three groups of proteins featured most prominently. Symptomatic WNF and WNE patients at the acute time point showed lower abundance of 3 proteins (B2M, APOA1, and APOA2; red box) relative to the levels observed in the asymptomatic participants which all equalize at the 3 month time point. This includes beta 2-microglobulin (B2M), a component of class I major histocompatibility complexes, which is known to be elevated in viral infections.[72] A group of four proteins (C8A, FBLN1, APOD, and TDRD1; green box) demonstrated elevated levels in the serum of both acutely infected asymptomatic and WNF patients but were significantly lower in WNE samples (although some heterogeneity is noted in Asymp 1 at the acute time point).

The highest number of significantly different serum proteins was a group of 12 proteins which were elevated specifically in WNE symptomatic patients at the acute time point (IGFALS, APOE, VTN, SAA1, C9, SERPINA3, APOA4, HP, CD14, APOL1, GC, and PLG; blue box). These markers include GC (vitamin D-binding protein); plasminogen (PLG), an acute phase reactant; and apolipoprotein A1 (APOL1) which responds to inflammatory cytokines and is involved in autophagy,[73] and CD14, the soluble form of the monocyte surface marker which is an indicator of monocyte activation consistent with CyTOF profiles noted previously in symptomatic participants. Elevated sCD14 is associated with inflammation and viral infections.[74] Expression levels of these proteins decreased at Month 3 and further declined at the Year 1 time points. Our study also identified elevated levels in symptomatic participants of the serum protein IGFALS, insulin-like growth factor binding protein acid-labile subunit, which has recently been shown to facilitate ubiquitination of signaling mediators IRAK1 and TRAF6 to inhibit influenza viral replication and in addition is a sensitive biomarker of COVID-19 infection.[75,76] This proteomic profile highlights important elements in the host response to acute WNV infection and identifies differences between the severity groups, specifically reflecting higher systemic inflammation in symptomatic participants.

Interactions between metabolic and immune pathways are incompletely understood but are a critical element of host response. Circulating metabolites are a link that both reflect systemic conditions as well as modulating cell states. To identify metabolic pathways that change in response to infection with WNV, we conducted untargeted LC-MS-based metabolomics on serum samples from our cohort. From a small sample set (n = 11 participants, n = 22 samples), we conducted an exploratory evaluation and identified 641 metabolites across all participants. When we compared acute and Month 3 time points for all participants together, we detected differentially abundant metabolites with 42 increased and 35 decreased (Figure 5A). In this longitudinal comparison, the biggest differences were detected in 5 glycerophospholipids of which 4 were more abundant at acute infection. These metabolites include lysophosphatidylethanolamine (LPE), lysophosphatidylcholine (LPC), and phosphatidylethanolamine (PE), which are amphipathic lipids in lipid bilayers that play a role in immune activation (Figure 5A, C22:6 LPE, C22:5 LPC, C22:6 LPC. C38:6 PE). Elevations in LPE have previously been correlated with higher disease activity in rheumatoid arthritis suggesting they may be important for immune activity.[77] In addition, 3 members of the alpha-linolenic acid and linoleic acid metabolism pathway were higher in acute infection and metabolites in the bile acid biosynthesis pathway showed an increased abundance at Month 3 (Figure 5A).

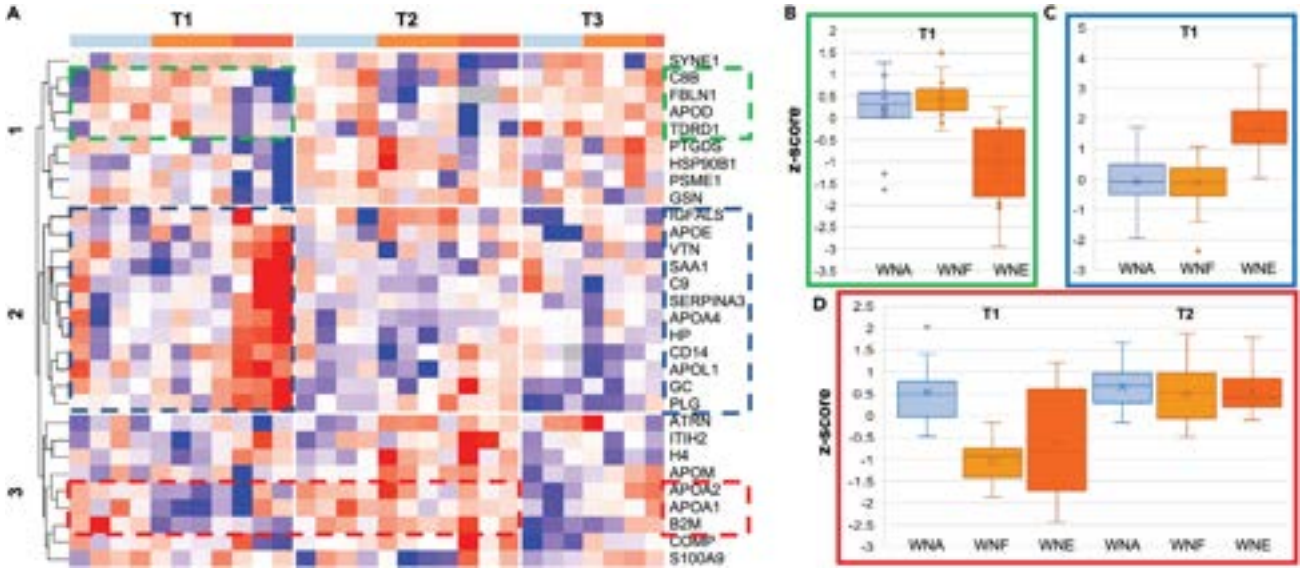

Figure 4. Plasma proteomics investigation in WNV infection

Serum proteins were assessed using MStern blotting followed by a highly multiplexed targeted MRM LC-MS experiment.

(A–D) (A) Hierarchical clustering-based heatmap showing the significant proteins (ANOVA; $p < 0.05$) based on the disease severity across the different time points. Protein groups of interest are indicated by green, blue and red boxes. Box/whisker plots of the z-scores across all proteins and participants indicated by the green (B), blue (C) and red (D) boxes. See also Table S4.

We also compared metabolic profiles between samples from asymptomatic participants (n = 8) and symptomatic patients (n = 14) to highlight any changes associated with clinical severity. When we compared subject groups, we detected distinct patterns of differentially abundant metabolites with 35 increased and 70 decreased metabolites in symptomatic compared to asymptomatic participants. WNV symptomatic participants exhibited the highest increase in triacylglycerols (C46:3 TAG, C46; 2 TAG, C44:1 TAG, C44:2 TAG), while asymptomatic participants showed an increase abundance of histidine, pyrimidine, and tyrosine metabolites (Figure 5B). A higher abundance of histidine in asymptomatic participants is consistent with previous reports of an anti-inflammatory effect.[77]

Integrative analysis by multi-omics factor analysis (MOFA)

Each of the multi-dimensional profiling platforms (cellular, transcriptional, proteomic, and metabolomic profiling) identified distinct factors that exhibit significant associations with the time points and disease groups and which may contribute to efficacy of responses and severity of WNV infection. A key question is whether individual elements, which alone may provide limited specificity or biological insight, may be highly correlated across platforms and interact together to drive the immune response. Thus, considering features derived from the combined systems analysis may identify signatures critical to clinical outcome. For more insight into immune components, we integrated the data from all the assay platforms using a joint dimension reduction with multi-omics factor analysis (MOFA) based on features from our four different assays (CyTOF, Seq-Well, proteomics and metabolomics).[78,79] MOFA identified 7 multi-omic factors (maximum number of factors suggested by MOFA) which explain 46.4% of the variance averaged over assays. For each factor, we performed two-way ANOVA analysis and assessed whether infection time point and disease severity explain additional variation in the MOFA factor scores across participants (Table S5). We focus on MOFA factor 1 which demonstrated the most significant difference across time points (p value 7.90E-07, adjusted p value 5.50E-06) and MOFA Factor 5 (p value 2.20E-02, adjusted p value 1.60E-01) with the strongest difference distinguishing between the multiple severity groups.

We found MOFA factor 1 was significantly associated with the time points. MOFA factor 1 was highest at the acute time point and decreased over time in the convalescent samples (Figure 6A, p value of 7.9E-07, adjusted p value of 5.5E-5). The top features of MOFA factor 1 are from CyTOF and Seq-Well and include 17 cell type frequencies and 109 cell type functional marker combinations from CyTOF, 10 proteins, 15 metabolites, and 1,464 genes (Table S6). MOFA factor 1 expression level represents a state with elevated frequencies of activated $CD8^+$ and $CD4^+$ T cells as well as lower levels of NK cells, Tregs, and DCs. Increased frequency of $CD8^+$ T cells and decreased frequency of NK cells at the acute time point was also identified when analyzing the cell frequencies directly (Figure 1). Functional markers identified in MOFA factor 1 and elevated at the acute time point include the leukocyte adhesion marker CD62L (L-selectin) on monocytes, DCs, NKs, $CD4^+$, and $CD8^+$ T cells; elevated expression of IFNγ in DCs, B cells, and $CD8^+$ T cells; elevated immune regulator CD279 on granulocytes and T and B cells; elevated chemokine receptors CCR4 on monocytes and $CD8^+$ T cells and CCR7 on $CD4^+$ and $CD8^+$ T cells. MOFA factor 1 also included lower expression of checkpoint inhibitor CD152 on $CD4^+$ T cells and NK cells. The most significant protein signature in MOFA factor 1 was complement and coagulation cascades (WikiPathway 3.66e-04). MOFA factor 1 includes serum proteins PROS1, involved in coagulation and

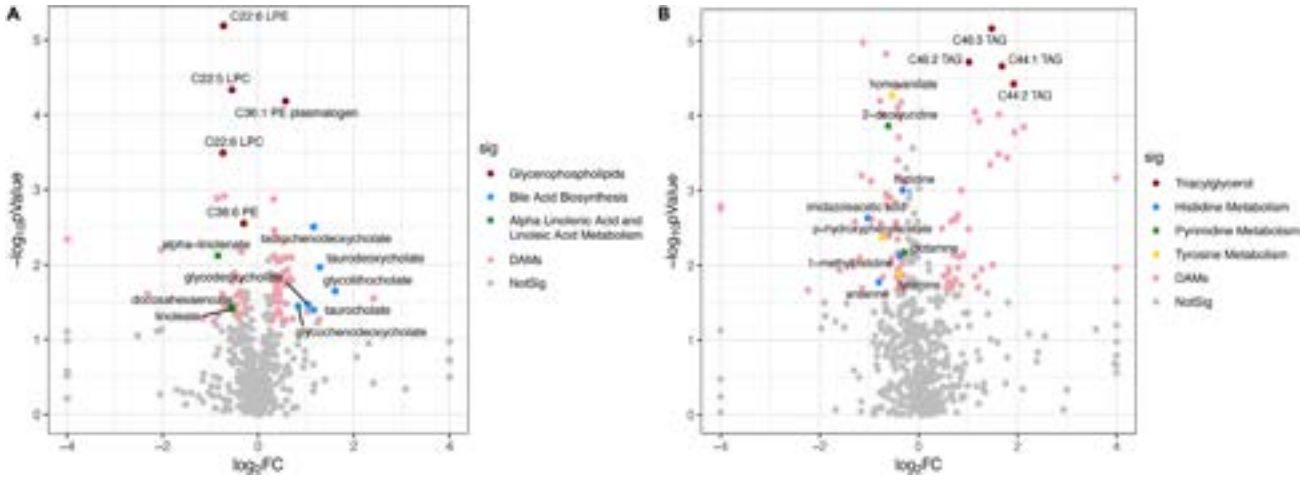

Figure 5. Differentially abundant metabolites in WNV infection

Serum metabolites were assessed using LC-MS, median normalized and log transformed.

(A and B) Differentially abundant metabolites (DAMs) are shown in volcano plots comparing (A) time point (Month 3 vs. Day 1) for all subjects at and (B) symptom severity (symptomatic n = 7 vs. asymptomatic n = 4). Colored points represent DAMs with absolute value of fold change (FC) ≥1.2, p value <0.05 (one-way ANOVA), and FDR (Storey's q-value) < 0.2 (A) or <0.05 (B).

clearance of apoptotic cells as a ligand for receptor tyrosine kinases TAM receptors (Tyro3, Axl, and Mer)[80] and APOA4, APOL1, which have primary roles in lipid transfer as well as immune-responsive role in autophagy, and SERPING1 which acts to inhibits the complement cascade. Among the metabolomic profiles, MOFA factor 1 identified decreased abundance at acute infection of enriched metabolites in the steroid biosynthesis pathway and spermidine pathway, ribothymidine and methylthioadenosine, reported to have anti-apoptotic effects,[81] and C34:2 PC plasmalogen, C36:1 PE plasmalogen, membrane lipids associated with immune signaling and protective against reactive oxygen species.[82]

In particular, B cell receptor (BCR) signaling was found to be the top enriched pathway among the 1,464 genes for MOFA factor 1 (WikiPathway, 2.01e-05), although our module-based Seq-Well analysis did not identify a B cell module. Notably, in CyTOF, the frequency of memory B cells was significantly elevated at the acute time point for all participants (Figure 1B, $p < 0.01$). These results highlight importance of B cells in early responses to infection with WNV. Since the MOFA analysis is based on global average gene expression across all cells regardless of cell types, we sought to determine whether the B cell signaling identified in MOFA factor 1 was due to changes in cell frequency or reflected activation within the B cell population. Therefore, we re-examined genes in the Seq-Well data related to BCR signaling (134 BCR signaling genes identified by two databases (WikiPathway (n = 97) and KEGG (n = 81) including 44 shared genes) to investigate whether there was differential gene expression within the B cell populations. We examined expression for the 22 genes in the BCR signaling pathway included in MOFA factor 1, comparing B cells in the 18 pairs of severity states and time points. Strikingly, we found differential expression for 21 of 22 genes in at least one condition (p value <0.01, Wilcoxon rank-sum test) and highly significant differential expression for 16 of 22 (p value <0.001). Particularly interesting are 3 genes elevated in the acute samples that are significant across time and severity groups (Figure 6B): *RAPGEF1*, a guanine nucleotide exchange factor involved in signal transmission and lineage-specific differentiation[83]; *LYN* and *REL*, activating src family tyrosine kinases. In contrast, *PPP3CA*, a calcineurin protein which activates T cells, showed higher expression during convalescence, particularly in the symptomatic cases reflecting their higher inflammatory status. For a subset of samples with sufficient cell numbers to support a separate analysis, we identified significant differences within plasma B cells specifically and similarly found lower expression at the acute time point for expression of *HCLS1* and *PPP3CA* (p value <0.01) consistent with expected kinetics of plasma cells in early response and the differential levels for B cell subsets.

We found a significant severity-related effect in MOFA factor 5 (Figure 6C, factor 5, ANOVA p value of 2.3E-2, adjusted p value 0.16) with asymptomatic participants having higher expression of MOFA factor 5. In addition, MOFA factor 5 also showed a difference across time points (3.90E-3, adjusted p value 2.30E-02). Further, the trajectory of paired MOFA factor 5 scores for each individual, calculated as the difference between levels at acute and 3 month time points, were significantly different between severity groups, with the symptomatic group increasing compared to asymptomatic groups (Figure 6D p value of 1.7E-3, adjusted p value of 1.2E-2; Wilcoxon rank-sum test). The top features of MOFA factor 5 are balanced between CyTOF, Seq-well, and proteomics and include 2 cell type frequencies and 4 functional marker combinations from CyTOF, 14 proteins, 14 metabolites, and 744 genes (Table S7). Asymptomatic participants had higher expression of MOFA factor 5 at the acute time point which represents an immune state of lower frequency of total B cells, and lower pro-inflammatory signaling pathways including reduced TGFβ in $CD8^+$ T cells, pSTAT1 in mDCs, and pSTAT5 in $CD4^+$ T cells. Serum proteins with elevated levels in MOFA factor 5 include components of the complement and coagulation cascades, e.g., complement protein C1S, Alpha2-HS glycoprotein (AHSG), involved in endocytosis and previously associated with severity in a murine model of WNV.[84] MOFA factor 5 includes reduced levels of complement protein C1QB and APOC3 which has a primary role in triglyceride transport but may also be relevant in inflammation as a

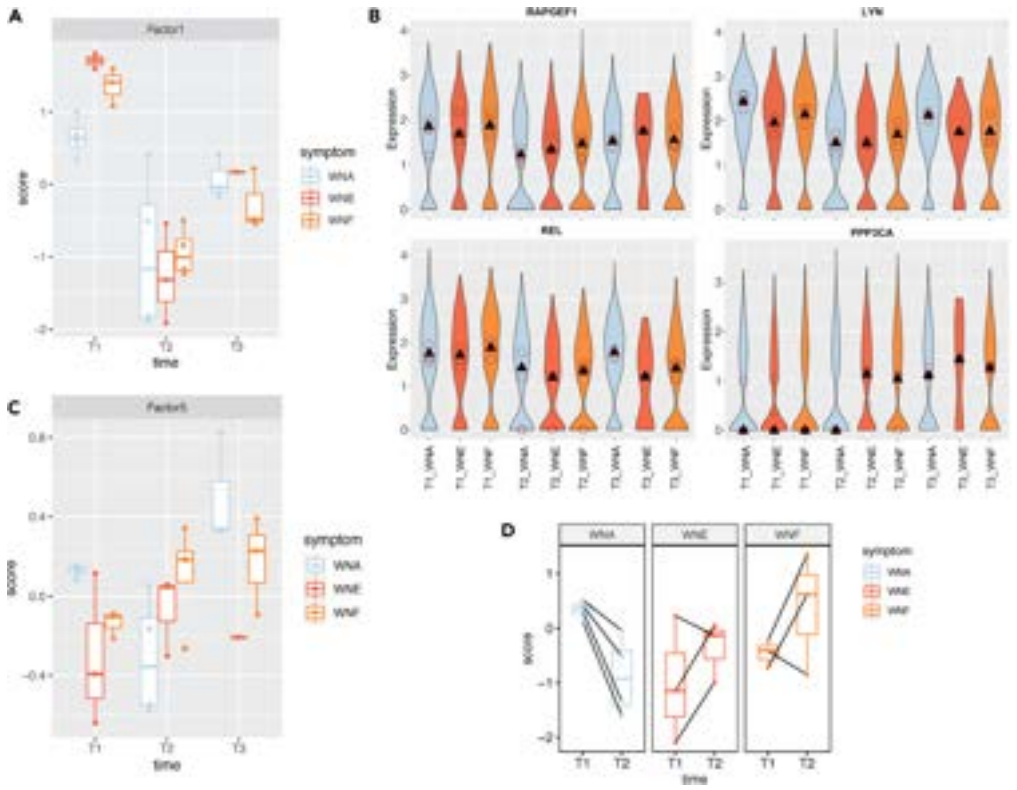

Figure 6. Multi-Omics Factor Analysis (MOFA)

Data from all the assay platforms were integrated using a joint dimension reduction with Multi-Omics Factor Analysis (MOFA).

(A) Box/whisker plots for MOFA factor 1 across time and severity groups. A two-way ANOVA test suggests a strong difference in Factor 1 (p = 8E-07) after accounting for across disease group variability.

(B) Expression of BCR signaling genes in B cell subsets across time points and severity groups. The triangles and circles represent median values as in Figure 3C.

(C) Box/whisker plot across time and severity groups for MOFA factor 5. A two-way ANOVA test suggests mild differences in Factor 5 (p = 4E-3) across times and across disease groups (p = 2E-2). A Wilcoxon rank-sum test suggests that both asymptomatic and symptomatic groups show differences at the acute time point (p = 8E-3).

(D) Box/whisker paired-plot on changes between T1 and T2 for different participants. A Wilcoxon rank-sum test suggests that asymptomatic and symptomatic groups show differences regarding the trajectory from T1 to T2 (p = 1E-3). See also Tables S5–S7.

competitor of anti-inflammatory apoE.[85,86] Metabolites identified in MOFA factor 5 were propanoate metabolism which is important in mitochondrial energy metabolism,[87] and alpha-hydroxybutyrate, an alternate energy source and regulator of cellular signaling.[88] MOFA factor 5 transcriptional features were highly enriched in mRNA processing (WikiPathway 1.8e-05).

DISCUSSION

WNV infection can be severe or fatal for only a minority of individuals. In this study, we for the first time employed a longitudinal multi-omic approach beginning with acute infection to define early cellular and molecular signatures corresponding to severe WNV infection. Although the sample size is small, insights we gained from defining effective immune responses may inform future investigation of specific cellular mechanisms and preventative and therapeutic approaches to mitigate severe WNV in susceptible people. We took advantage of an unusual population of acutely infected but asymptomatic individuals and interrogated immune responses to identify individual variations that may contribute to infection severity. We applied powerful single-cell approaches to interrogate immune responses at acute infection and through convalescence. Following multiple measures over time from the same study participants reduces variation in our assays and supports development of the trajectory of infection response. Through an integrated analysis comparing multiple immune components in asymptomatic and symptomatic cases, we defined elements characterizing different clinical outcomes.

An unexpected finding from our study is the similarity of responses in the study participants. Across severity groups, we detected significant alterations in cell frequencies and functions, transcriptional, proteomic, and metabolomic pathways, reflecting that WNV is a potent virus which evokes strong immune responses. We have previously quantified antibody responses to WNV proteins (envelope and non-structural proteins 1 and 5) and assessed humoral response to WNV on a single-cell and repertoire level and shown no significant differences between groups whether they experienced asymptomatic or severe infection.[33,89] Changes in cell frequencies—such as elevated innate immune PMN and monocytes at acute infection, and the expansion of effector $CD4^+$ (Temra) cells at Month 3 and Year 1—were similar across severity

groups. We showed differences, however, in cellular functional responses with relatively elevated levels of inflammatory cytokines (TNF, IL-8, and IFNγ) and signaling mediators (phospho STAT3 and phospho STAT5) in the group with severe WNV infection. The elevated levels of activated $CD8^+$ T cells at Day 1 are expected in symptomatic participants given the important role for activated $CD8^+$ T cells in response to viral infections, related to their recognized functional activities in viral killing and clearance and production of inflammatory mediators. However, our data reveal comparable increased frequencies in asymptomatic donors which might not have been predicted given the absence of clinical symptoms. In transcriptional responses, similarly, all participants demonstrated elevated transcription of cDC, $CD8^+$ T cell, and $CD14^+$ monocyte gene signatures at acute infection which declined by Month 3 and Year 1. The slight differences in cell type frequencies between the CyTOF and Seq-Well platforms, or between transcriptional and proteomic measurements, may be due to mRNAs which are not transcribed, or protein markers which may be undetectable or shed or secreted on activation, or to differences in whole blood vs. PBMC samples. We also identified particularly notable differences in gene modules in non-classical $CD16^+$ monocytes of asymptomatic participants, a subset specialized for wound healing and anti-viral responses.[90] In particular, the IFN response is a very important element of anti-viral activity and higher expression of these genes in asymptomatic participants suggests the early expression of these pathways may control infection effectively. In addition, those features of the asymptomatic response to acute infection would be expected to increase viral clearance and overall lower the degree of inflammation in asymptomatic donors. Through a ligand-target analysis of cell-type and state based on average signals of individuals, we identified markers of interest enriched during infection and in different disease trajectories to ground generated gene-sets in known cellular interactions.

We broadened our examination of immunity by profiling serum proteins and metabolites, identifying significant differences longitudinally in all study participants as well as specific components that distinguish severity groups. In particular, these analyses, while limited by sample size, highlighted elevated serum levels in more severely ill WNV participants of acute phase reactants and inflammatory processes including the complement and coagulation pathways,[71] and that serum levels of some proteins remained elevated over 3 months, consistent with other clinical observations.[91] Notably, insulin-like growth factor binding protein acid-labile subunit (IGFALS) was also higher in more severely ill WNV study participants which may reflect its role inhibiting viral infection.[75,76] Asymptomatic participants had elevated levels of complement and coagulation, and elevated levels of the metabolic pathways enhancing energy production. These elevated proteins are consistent with acute serum proteome responses in Lyme disease, another arthropod-borne infection, although microbiologically distinct and transmitted by a different vector, suggesting similar immune activation.[70] Regulation of those proteins may be beneficial or predictive of an improved clinical trajectory. Considering the importance of cytokines in immune response and given our transcriptomics data, we note that there are 8 cytokines with both protein abundance and gene expression data (HSPB1, ICAM1, IGHD, ITIH4, LBP, PF4, PPBP, and VCAM1) and that their protein-gene correlation is generally poor with Pearson correlations between 0.245 (ITIH4) and 0.286 (HSPB1). Many cytokines of immune response have local action, so may not be seen in the blood. In addition, they have such low concentrations in the blood (e.g., interferons) that they are not detected on typical proteomics platforms. There is also a detection limit with bulk proteomics compared to single-cell transcriptomics. In general, there is little correlation between gene and protein levels in complex systems due to either post-transcriptional or post-translation regulation.[92]

With respect to serum metabolites, all groups at acute infection showed elevated levels of glycerophospholipid, which is associated with immune activation and has recently been associated with inflammatory responses to influenza vaccination.[93] Elevations at Month 3 may indicate a trajectory toward resolution of inflammation because bile acids have a regulatory role in inhibiting inflammasome activation.[94] Furthermore, we detected an increased abundance of anti-inflammatory histidine metabolites in asymptomatic individuals. These differences suggest increased regulation of metabolic pathways in asymptomatic participants during acute WNV infection which may contribute to the improved clinical trajectory. This is consistent with cell functional markers and transcriptional targets, showing elevated levels of inflammatory pathways in each omics platform in symptomatic participants is likely relevant for disease severity. Understanding the milieu of immune cells enriches our understanding of the response to infection and provides additional evidence of inflammatory differences distinguishing severity groups.

With this data resource as input, we applied multi-omics factor analysis (MOFA) to generate salient hybrid features derived from the combined systems analyses. With the integrated data from all the assay platforms, several distinct findings emerged. As noted in each individual assay platform, there were many elements of response to WNV infection which were shared by all severity groups. Despite engagement of these responses, individuals show highly divergent clinical outcomes. The coordinated elements identified via integrated MOFA multi-omics modeling provide mechanistic insight and may identify signatures critical to clinical outcome. Specifically, MOFA factor 1 identified significant elements associated with the time course trajectory of infection with a focus on B cells that correlates with cell frequency data and is consistent with higher gene expression levels at the acute time point, supported by the gene set enrichment of BCR signaling. This response may be critical, with early activity of B cells having an important protective role in infections in both asymptomatic and symptomatic subjects. Studies in the mouse model showed that B cells were essential for resistance to WNV infection.[95] We have previously shown that antibody levels examined in convalescence were not significantly different between asymptomatic and severely ill participants and did not predict clinical severity,[33,89] and we similarly found strong anti-WNV E responses by immunoblot from all participants in the current study. Thus the importance of the B cell transcriptional signatures as identified in the MOFA analysis may be related to other B cell roles and interactions besides secretion of antibody.

Through our analysis we determined that effective immune responses in asymptomatic donors include an activated immune status involving cell types and pathways that initially controlled pro-inflammatory innate immune cell activation and elevated numbers of Tregs noted in MOFA factor 1. This observation is consistent with previous measures of Tregs in infection with WNV in studies restricted to symptomatic participants.[30] Our MOFA analysis identifies an immune state combining multiple immune components and suggests that less severe WNV infection is associated with a combined immune state of reduced proinflammatory activity and elevated levels of B2m, ApoA1, Apo A2

proteins. While very few individual features independently can distinguish disease severity groups, especially in a small cohort, with the combined activity of many potentially small contributions of several immune components, MOFA identifies an immune state whose joint effect is more significant for separating the disease cohorts. In addition, the key cellular immune responses and metabolic pathways of MOFA factor 5 identify a constellation of critical immune elements which contribute to successful responses. The significance of opposite trajectories of MOFA factor 5 between severity groups from acute to Month 3 time points suggests that the different immune profiles evident between clinical groups during acute infection may drive different trajectories for clinical outcome.

Our study cohort is limited by enrollment size which is dependent on variations in infection frequency at our recruitment site (Houston, TX) and was conducted during disruptive seasons which included Hurricane Harvey as well as the COVID-19 pandemic. Focusing only on WNV-exposed individuals allows us to assess the determinants of different responses to the virus. Healthy uninfected individuals, while easier to recruit, are not appropriate controls for this study, as their anti-WNV efficiency is undefined prior to infection. Although WNV infections are typically asymptomatic,[33] it is unknown how individual uninfected controls would respond to infection, making such a group incompatible with our goal of defining molecular characteristics that differentiate asymptomatic and symptomatic infection responses. Our inclusion of a convalescent time point at Year 1 served as a proxy to healthy conditions. Beyond the distinct immune elements identified here, additional factors and mechanistic conclusions may be revealed in a study using a larger cohort and where participant sex could be considered, mild fever and severe neurologic subjects could be distinguished, and detailed medication history could be collected from asymptomatic participants. In addition, WNV is a vector-mediated infection, and our study does not specifically examine the impact of mosquito salivary components. The host immune response to the vector has recently been highlighted as contributing to resistance in some tick-borne infections[96] and shows promising protection with anti-mosquito vaccine or interventions directed at viral proteins such as non-structural (NS)-1.[97]

Our approach, including a longitudinal stratified profiling plan and MOFA analysis, offers a data resource of acute human viral infection and a model for multifactorial immune inquiry. Through this in-depth profile, we uncovered distinctions between patients who have very dramatic differences in clinical outcome. Medicine is developing a rich understanding of cellular immune pathways and how they may be leveraged for clinical advantage. With an additional understanding of the proteomic and metabolomic datasets, the profiles provide potentially actionable biomarkers for vulnerable individuals. Beyond prognosis, defining measurable differences in immune response between disease trajectories in a larger subject cohort can inform targeted approaches to prevent and/or treat WNV infection, including selective immunomodulation.

The observation of the combined immune state with joint molecular effects could not be addressed in previous studies examining only severely infected patients or from profiles of convalescent cohorts enrolled after recovery from infection.[30,31,98] Although stratified by disease severity, they were evaluated after recovery from acute illness when differences in initiation of B cell responses were not evident.[33,89] The mechanisms identified here in profiles of asymptomatic study participants may be useful for understanding mechanisms of pathogenesis for other viral infections as well, particularly for related flaviviruses such as Zika and dengue viruses.[39,99,100] Finally, considering the fact that there is no WNV vaccine for humans,[101,102] our study using systems immunology approaches may have an implication for WNV vaccine development too. In particular, our single-cell immune profiling and gene modules could contribute to vaccine design by inferring cell type-specific susceptibility to infection.[103]

Limitations of the study

First, the cohort size of our study was small as it depends on infection frequency and was conducted during disruptive seasons which included Hurricane Harvey as well as the COVID-19 pandemic. Second, WNV being a vector-mediated infection, immunity to the mosquito vector may play a role which our study did not examine. Third, our study did not address the recent finding that auto-antibodies neutralizing IFN-α and/or IFN-ω were found with greater frequency in patients with severe WNV infection.[18,19] Finally, our enrollment criteria provide limited related health information for the participants, especially the asymptomatic donors.

STAR★METHODS

Detailed methods are provided in the online version of this paper and include the following:

- KEY RESOURCES TABLE
- RESOURCE AVAILABILITY
  - Lead contact
  - Materials availability
  - Data and code availability
- EXPERIMENTAL MODEL AND STUDY PARTICIPANT DETAILS
  - Human study participants and ethics statement
- METHOD DETAILS
  - Sample collection and cell isolation
  - Cell labeling and mass cytometry acquisition
  - CyTOF data processing and analysis
  - Single cell transcriptional assays
  - scRNA-seq raw data processing

- scRNA-seq cell type identification
- Differential gene module discovery
- Intercellular communication predictions
- Proteomics
- Metabolomics
- Metabolomics data processing
- Multi-omics data integration

● QUANTIFICATION AND STATISTICAL ANALYSIS

SUPPLEMENTAL INFORMATION

Supplemental information can be found online at https://doi.org/10.1016/j.isci.2023.108387.

ACKNOWLEDGMENTS

This work was supported in part by awards from the NIH/NIAID Human Immunology Project Consortium (HIPC) grant (AI089992 to RRM, DAH, SHK, JCL, AKS; AI118608 to BF, KKS, HS, OL), the Koch Institute Support (core) NIH Grant P30-CA14051 from the National Cancer Institute, and the Claude D. Pepper Older Americans Independence Center from the NIH/NIA (P30AG021342) to BvW. The *Precision Vaccines Program* is supported in part via the Department of Pediatrics at Boston Children's Hospital. The authors gratefully acknowledge the valuable contributions of the HIPC group and Yale School of Medicine colleagues and core facilities (Yale CyTOF core and Yale Center for Genome Analysis), Ms. Jeanne Ruff and Ms. Allison Lino for assistance with the Houston West Nile Cohort, Dr. Susan N. Rossman and members of the Gulf Coast Regional Blood Bank for identifying asymptomatic participants, and all the study participants. The funders had no role in study design, data collection and analysis, decision to publish, or preparation of the manuscript.

AUTHOR CONTRIBUTIONS

Conceived and planned the study, D.A.H., S.H.K., R.R.M., and K.O.M. Performed experiments, Y.Z., I.F., X.W., H.K., C.H.C., B.F., and K.K.S. Analyzed and visualized data, H.J.L., Y.Z., I.F., S.M., X.W., B.V.W., C.B.C., H.K., C.H.C., B.F., K.K.S., O.L., H.S., A.K.S., L.G., S.H.K., and R.R.M. All authors contributed to writing and reviewing the manuscript. R.R.M. coordinated the contribution of all authors.

DECLARATION OF INTERESTS

A.K.S. reports compensation for consulting and/or SAB membership from Merck, Honeycomb Biotechnologies, Cellarity, Repertoire Immune Medicines, Ochre Bio, Third Rock Ventures, Hovione, Relation Therapeutics, FL82, and Dahlia Biosciences. J.C.L., A.K.S. and the Massachusetts Institute of Technology have filed patents related to the single-cell sequencing methods used in this work. J.C.L. has interests in Sunflower Therapeutics PBC, Honeycomb Biotechnologies, OneCyte Biotechnologies, Alloy Therapeutics, QuantumCyte, and Repligen. J.C.L.'s interests are reviewed and managed under Massachusetts Institute of Technology's policies for potential conflicts of interest. R.J.X. is a cofounder of Celsius Therapeutics and Jnana Therapeutics. S.H.K. receives consulting fees from Peraton.

INCLUSION AND DIVERSITY

We support inclusive, diverse, and equitable conduct of research.

Received: May 30, 2023
Revised: October 4, 2023
Accepted: October 27, 2023
Published: November 2, 2023

REFERENCES

1. Bai, F., Thompson, E.A., Vig, P.J.S., and Leis, A.A. (2019). Current Understanding of West Nile Virus Clinical Manifestations, Immune Responses, Neuroinvasion, and Immunotherapeutic Implications. Pathogens *8*, 193. https://doi.org/10.3390/pathogens8040193.
2. Ronca, S.E., Ruff, J.C., and Murray, K.O. (2021). A 20-year historical review of West Nile virus since its initial emergence in North America: Has West Nile virus become a neglected tropical disease? PLoS Negl. Trop. Dis. *15*, e0009190. https://doi.org/10.1371/journal.pntd.0009190.
3. Hadfield, J., Brito, A.F., Swetnam, D.M., Vogels, C.B.F., Tokarz, R.E., Andersen, K.G., Smith, R.C., Bedford, T., and Grubaugh, N.D. (2019). Twenty years of West Nile virus spread and evolution in the Americas visualized by Nextstrain. PLoS Pathog. *15*, e1008042. https://doi.org/10.1371/journal.ppat.1008042.
4. Petersen, L.R. (2019). Epidemiology of West Nile Virus in the United States: Implications for Arbovirology and Public Health. J. Med. Entomol. *56*, 1456–1462. https://doi.org/10.1093/jme/tjz085.
5. Centers for Disease Control and Prevention, C.D.C (2020). West Nile Virus, Final Cumulative Maps & Data for 1999–2019. https://www.cdc.gov/westnile/statsMaps/cumMapsData.html.
6. Ronca, S.E., Murray, K.O., and Nolan, M.S. (2019). Cumulative Incidence of West Nile Virus Infection, Continental United States, 1999-2016. Emerg. Infect. Dis. *25*, 325–327. https://doi.org/10.3201/eid2502.180765.
7. Suthar, M.S., and Pulendran, B. (2014). Systems analysis of West Nile virus infection. Curr. Opin. Virol. *6*, 70–75. https://doi.org/10.1016/j.coviro.2014.04.010.

8. Montgomery, R.R., and Murray, K.O. (2015). Risk factors for West Nile virus Infection and disease in populations and individuals. Expert Rev. Anti. Infect. Ther. *13*, 317–325.
9. Loeb, M., Eskandarian, S., Rupp, M., Fishman, N., Gasink, L., Patterson, J., Bramson, J., Hudson, T.J., and Lemire, M. (2011). Genetic variants and susceptibility to neurological complications following West Nile virus infection. J. Infect. Dis. *204*, 1031–1037.
10. Bigham, A.W., Buckingham, K.J., Husain, S., Emond, M.J., Bofferding, K.M., Gildersleeve, H., Rutherford, A., Astakhova, N.M., Perelygin, A.A., Busch, M.P., et al. (2011). Host genetic risk factors for West Nile virus infection and disease progression. PLoS One *6*, e24745.
11. Cahill, M.E., Loeb, M., DeWan, A.T., and Montgomery, R.R. (2020). In-depth analysis of Genetic Variation Associated with Severe West Nile Viral Disease. Vaccines *8*, 744. https://doi.org/10.3390/vaccines8040744.
12. Suthar, M.S., Diamond, M.S., and Gale, M., Jr. (2013). West Nile virus infection and immunity. Nature reviews *11*, 115–128. https://doi.org/10.1038/nrmicro2950.
13. van Tol, S., Atkins, C., Bharaj, P., Johnson, K.N., Hage, A., Freiberg, A.N., and Rajsbaum, R. (2020). VAMP8 Contributes to the TRIM6-Mediated Type I Interferon Antiviral Response during West Nile Virus Infection. J. Virol. *94*, e01454-19. https://doi.org/10.1128/JVI.01454-19.
14. Luo, H., Winkelmann, E.R., Zhu, S., Ru, W., Mays, E., Silvas, J.A., Vollmer, L.L., Gao, J., Peng, B.H., Bopp, N.E., et al. (2018). Peli1 facilitates virus replication and promotes neuroinflammation during West Nile virus infection. J. Clin. Invest. *128*, 4980–4991. https://doi.org/10.1172/JCI99902.
15. Suthar, M.S., Brassil, M.M., Blahnik, G., McMillan, A., Ramos, H.J., Proll, S.C., Belisle, S.E., Katze, M.G., and Gale, M., Jr. (2013). A systems biology approach reveals that tissue tropism to West Nile virus is regulated by antiviral genes and innate immune cellular processes. PLoS Pathog. *9*, e1003168. https://doi.org/10.1371/journal.ppat.1003168.
16. Graham, J.B., Swarts, J.L., Thomas, S., Voss, K.M., Sekine, A., Green, R., Ireton, R.C., Gale, M., and Lund, J.M. (2019). Immune Correlates of Protection From West Nile Virus Neuroinvasion and Disease. J. Infect. Dis. *219*, 1162–1171. https://doi.org/10.1093/infdis/jiy623.
17. Stone, A.E.L., Green, R., Wilkins, C., Hemann, E.A., and Gale, M., Jr. (2019). RIG-I-like receptors direct inflammatory macrophage polarization against West Nile virus infection. Nat. Commun. *10*, 3649. https://doi.org/10.1038/s41467-019-11250-5.
18. Gervais, A., Rovida, F., Avanzini, M.A., Croce, S., Marchal, A., Lin, S.-C., Ferrari, A., Thorball, C.W., Constant, O., Le Voyer, T., et al. (2023). Autoantibodies neutralizing type I IFNs underlie West Nile virus encephalitis in ~40% of patients. J. Exp. Med. *220*, e20230661. https://doi.org/10.1084/jem.20230661.
19. Lin, S.-C., Zhao, F.R., Janova, H., Gervais, A., Rucknagel, S., Murray, K.O., Casanova, J.-L., and Diamond, M.S. (2023). Blockade of interferon signaling decreases gut barrier integrity and promotes severe West Nile virus disease. Nat. Commun. *14*, 5973. https://doi.org/10.1038/s41467-023-41600-3.
20. Qian, F., Wang, X., Zhang, l., Lin, A., Zhao, H., Fikrig, E., and Montgomery, R.R. (2011). Impaired interferon signaling in dendritic cells from older donors infected in vitro with West Nile virus. J. Infect. Dis. *203*, 1415–1424.
21. Shaw, A.C., Goldstein, D.R., and Montgomery, R.R. (2013). Age-dependent dysregulation of innate immunity. Nat. Rev. Immunol. *13*, 875–887.
22. Pillai, P.S., Molony, R.D., Martinod, K., Dong, H., Pang, I.K., Tal, M.C., Solis, A.G., Bielecki, P., Mohanty, S., Trentalange, M., et al. (2016). Mx1 Reveals Innate Pathways to Antiviral Resistance and Lethal Influenza Disease. Science *352*, 463–466.
23. Molony, R.D., Nguyen, J.T., Kong, Y., Montgomery, R.R., Shaw, A.C., and Iwasaki, A. (2017). Aging Impairs Both Primary and Secondary RIG-I Signaling for Interferon Induction in Human Monocytes. Sci. Signal. *10*, eaan2392. https://doi.org/10.1126/scisignal.aan2392.
24. Molony, R.D., Malawista, A., and Montgomery, R.R. (2018). Reduced dynamic range of antiviral innate immune responses in aging. Exp. Gerontol. *107*, 130–135. https://doi.org/10.1016/j.exger.2017.08.019.
25. Goldberg, E.L., Shaw, A.C., and Montgomery, R.R. (2020). How inflammation blunts innate immunity in aging. In Vaccines for the Elderly: Present and Future, B. Weinberger, ed. (S. Karger Publishers), pp. 1–17. https://doi.org/10.1159/000504480.
26. Montgomery, R.R. (2017). Age-related alterations in immune responses to West Nile virus infection. Clin. Exp. Immunol. *187*, 26–34. https://doi.org/10.1111/cei.12863.
27. Cahill, M.E., Yao, Y., Nock, D., Armstrong, P.M., Andreadis, T.G., Diuk-Wasser, M.A., and Montgomery, R.R. (2017). West Nile virus Seroprevalence, Connecticut, USA, 2000-2014. Emerg. Infect. Dis. *23*, 708–710. https://doi.org/10.3201/eid2304.161669.
28. Qian, F., Goel, G., Meng, H., Wang, X., You, F., Devine, L., Raddassi, K., Garcia, M.N., Murray, K.O., Bolen, C.R., et al. (2015). Systems immunology reveals markers of susceptibility to West Nile virus infection. Clin. Vaccine Immunol. *22*, 6–16. https://doi.org/10.1128/CVI.00508-14.
29. Ramos, H.J., Lanteri, M.C., Blahnik, G., Negash, A., Suthar, M.S., Brassil, M.M., Sodhi, K., Treuting, P.M., Busch, M.P., Norris, P.J., and Gale, M., Jr. (2012). IL-1beta signaling promotes CNS-intrinsic immune control of West Nile virus infection. PLoS Pathog. *8*, e1003039. https://doi.org/10.1371/journal.ppat.1003039.
30. Lanteri, M.C., O'Brien, K.M., Purtha, W.E., Cameron, M.J., Lund, J.M., Owen, R.E., Heitman, J.W., Custer, B., Hirschkorn, D.F., Tobler, L.H., et al. (2009). Tregs control the development of symptomatic West Nile virus infection in humans and mice. J. Clin. Invest. *119*, 3266–3277.
31. Lanteri, M.C., Diamond, M.S., Law, J.P., Chew, G.M., Wu, S., Inglis, H.C., Wong, D., Busch, M.P., Norris, P.J., and Ndhlovu, L.C. (2014). Increased frequency of Tim-3 expressing T cells is associated with symptomatic West Nile virus infection. PLoS One *9*, e92134. https://doi.org/10.1371/journal.pone.0092134.
32. James, E.A., Gates, T.J., LaFond, R.E., Yamamoto, S., Ni, C., Mai, D., Gersuk, V.H., O'Brien, K., Nguyen, Q.A., Zeitner, B., et al. (2016). Neuroinvasive West Nile Infection Elicits Elevated and Atypically Polarized T Cell Responses That Promote a Pathogenic Outcome. PLoS Pathog. *12*, e1005375. https://doi.org/10.1371/journal.ppat.1005375.
33. Qian, F., Thakar, J., Yuan, X., Nolan, M., Murray, K.O., Lee, W.T., Wong, S.J., Meng, H., Fikrig, E., Kleinstein, S.H., and Montgomery, R.R. (2014). Immune markers associated with host susceptibility to infection with West Nile virus. Viral Immunol. *27*, 39–47.
34. Sekiguchi, D.R., Smith, S.B., Sutter, J.A., Goodman, N.G., Propert, K., Louzoun, Y., Rogers, W., and Luning Prak, E.T. (2011). Circulating lymphocyte subsets in normal adults are variable and can be clustered into subgroups. Cytometry B Clin. Cytom. *80*, 291–299. https://doi.org/10.1002/cyto.b.20594.
35. Whitney, A.R., Diehn, M., Popper, S.J., Alizadeh, A.A., Boldrick, J.C., Relman, D.A., and Brown, P.O. (2003). Individuality and variation in gene expression patterns in human blood. Proc. Natl. Acad. Sci. USA *100*, 1896–1901. https://doi.org/10.1073/pnas.252784499.
36. Brodin, P., and Davis, M.M. (2017). Human immune system variation. Nat. Rev. Immunol. *17*, 21–29. https://doi.org/10.1038/nri.2016.125.
37. Murray, K.O., Baraniuk, S., Resnick, M., Arafat, R., Kilborn, C., Shallenberger, R., York, T.L., Martinez, D., Malkoff, M., Elgawley, N., et al. (2008). Clinical investigation of hospitalized human cases of West Nile virus infection in Houston, Texas, 167-174. Vector Borne Zoonotic Dis. *8*, 167–174.
38. Gaudillière, B., Fragiadakis, G.K., Bruggner, R.V., Nicolau, M., Finck, R., Tingle, M., Silva, J., Ganio, E.A., Yeh, C.G., Maloney, W.J., et al. (2014). Clinical recovery from surgery correlates with single-cell immune signatures. Sci. Transl. Med. *6*, 255ra131. https://doi.org/10.1126/scitranslmed.3009701.
39. Zhao, Y., Amodio, M., Vander Wyk, B., Gerritsen, B., Kumar, M.M., van Dijk, D., Moon, K., Wang, X., Malawista, A., Richards, M.M., et al. (2020). Single cell immune profiling of dengue virus patients reveals intact immune responses to Zika virus with enrichment of innate immune signatures. PLoS Negl. Trop. Dis. *14*, e0008112. https://doi.org/10.1371/journal.pntd.0008112.
40. Finak, G., Langweiler, M., Jaimes, M., Malek, M., Taghiyar, J., Korin, Y., Raddassi, K., Devine, L., Obermoser, G., Pekalski, M.L., et al. (2016). Standardizing Flow Cytometry Immunophenotyping Analysis from the Human ImmunoPhenotyping Consortium. Sci. Rep. *6*, 20686. https://doi.org/10.1038/srep20686.
41. Bai, F., Kong, K.-F., Dai, J., Qian, F., Zhang, L., Brown, C.R., Fikrig, E., and Montgomery, R.R. (2010). A paradoxical role for neutrophils in the pathogenesis of West Nile virus. J. Infect. Dis. *202*, 1804–1812.
42. Hislop, A.D., Taylor, G.S., Sauce, D., and Rickinson, A.B. (2007). Cellular responses to viral infection in humans: lessons from Epstein-Barr virus. Annu. Rev. Immunol. *25*, 587–617. https://doi.org/10.1146/annurev.immunol.25.022106.141553.

43. Yao, Y., Strauss-Albee, D.M., Zhou, J.Q., Malawista, A., Garcia, M.N., Murray, K.O., Blish, C.A., and Montgomery, R.R. (2017). The natural killer cell response to West Nile virus in young and old individuals with or without a prior history of infection. PLoS One *12*, e0172625. https://doi.org/10.1371/journal.pone.0172625.
44. Ivetic, A., Hoskins Green, H.L., and Hart, S.J. (2019). L-selectin: A Major Regulator of Leukocyte Adhesion, Migration and Signaling. Front. Immunol. *10*, 1068. https://doi.org/10.3389/fimmu.2019.01068.
45. Lam, F.W., Vijayan, K.V., and Rumbaut, R.E. (2015). Platelets and Their Interactions with Other Immune Cells. Compr. Physiol. *5*, 1265–1280. https://doi.org/10.1002/cphy.c140074.
46. Debili, N., Robin, C., Schiavon, V., Letestu, R., Pflumio, F., Mitjavila-Garcia, M.T., Coulombel, L., and Vainchenker, W. (2001). Different expression of CD41 on human lymphoid and myeloid progenitors from adults and neonates. Blood *97*, 2023–2030. https://doi.org/10.1182/blood.v97.7.2023.
47. Pauken, K.E., Godec, J., Odorizzi, P.M., Brown, K.E., Yates, K.B., Ngiow, S.F., Burke, K.P., Maleri, S., Grande, S.M., Francisco, L.M., et al. (2020). The PD-1 Pathway Regulates Development and Function of Memory CD8(+) T Cells following Respiratory Viral Infection. Cell Rep. *31*, 107827. https://doi.org/10.1016/j.celrep.2020.107827.
48. Gorlé, N., Blaecher, C., Bauwens, E., Vandendriessche, C., Balusu, S., Vandewalle, J., Van Cauwenberghe, C., Van Wonterghem, E., Van Imschoot, G., Liu, C., et al. (2018). The choroid plexus epithelium as a novel player in the stomach-brain axis during Helicobacter infection. Brain Behav. Immun. *69*, 35–47. https://doi.org/10.1016/j.bbi.2017.12.010.
49. Gierahn, T.M., Wadsworth, M.H., 2nd, Hughes, T.K., Bryson, B.D., Butler, A., Satija, R., Fortune, S., Love, J.C., and Shalek, A.K. (2017). Seq-Well: portable, low-cost RNA sequencing of single cells at high throughput. Nat. Methods *14*, 395–398. https://doi.org/10.1038/nmeth.4179.
50. Stuart, T., Butler, A., Hoffman, P., Hafemeister, C., Papalexi, E., Mauck, W.M., 3rd, Hao, Y., Stoeckius, M., Smibert, P., and Satija, R. (2019). Comprehensive Integration of Single-Cell Data. Cell *177*, 1888–1902.e21. https://doi.org/10.1016/j.cell.2019.05.031.
51. Zhang, B., and Horvath, S. (2005). A general framework for weighted gene co-expression network analysis. Stat. Appl. Genet. Mol. Biol. *4*. Article17. https://doi.org/10.2202/1544-6115.1128.
52. Schroder, W.A., Hirata, T.D., Le, T.T., Gardner, J., Boyle, G.M., Ellis, J., Nakayama, E., Pathirana, D., Nakaya, H.I., and Suhrbier, A. (2019). SerpinB2 inhibits migration and promotes a resolution phase signature in large peritoneal macrophages. Sci. Rep. *9*, 12421. https://doi.org/10.1038/s41598-019-48741-w.
53. Cao, L., Yang, G., Gao, S., Jing, C., Montgomery, R.R., Yin, Y., Wang, P., Fikrig, E., You, F., Fikrig, E., and You, F. (2019). HIPK2 is necessary for type I interferon–mediated antiviral immunity. Sci. Signal. *12*, eaau4604. https://doi.org/10.1126/scisignal.aau4604.
54. Lang, R., and Raffi, F.A.M. (2019). Dual-Specificity Phosphatases in Immunity and Infection: An Update. Int. J. Mol. Sci. *20*, 2710. https://doi.org/10.3390/ijms20112710.
55. Nakano, N., Maeyama, K., Sakata, N., Itoh, F., Akatsu, R., Nakata, M., Katsu, Y., Ikeno, S., Togawa, Y., Vo Nguyen, T.T., et al. (2014). C18 ORF1, a novel negative regulator of transforming growth factor-beta signaling. J. Biol. Chem. *289*, 12680–12692. https://doi.org/10.1074/jbc.M114.558981.
56. Gonçalves, J., Sharma, A., Coyaud, É., Laurent, E.M.N., Raught, B., and Pelletier, L. (2020). LUZP1 and the tumor suppressor EPLIN modulate actin stability to restrict primary cilia formation. J. Cell Biol. *219*, e201908132. https://doi.org/10.1083/jcb.201908132.
57. Wabnitz, G., Balta, E., and Samstag, Y. (2017). L-plastin regulates the stability of the immune synapse of naive and effector T-cells. Adv. Biol. Regul. *63*, 107–114. https://doi.org/10.1016/j.jbior.2016.09.009.
58. Lusitani, D., Malawista, S.E., and Montgomery, R.R. (2003). Calprotectin, an abundant cytosolic protein from human polymorphonuclear leukocytes, inhibits the growth of *Borrelia burgdorferi*. Infect. Immun. *71*, 4711–4716.
59. Narasimhan, P.B., Marcovecchio, P., Hamers, A.A.J., and Hedrick, C.C. (2019). Nonclassical Monocytes in Health and Disease. Annu. Rev. Immunol. *37*, 439–456. https://doi.org/10.1146/annurev-immunol-042617-053119.
60. Fredman, G., and Tabas, I. (2017). Boosting Inflammation Resolution in Atherosclerosis: The Next Frontier for Therapy. Am. J. Pathol. *187*, 1211–1221. https://doi.org/10.1016/j.ajpath.2017.01.018.
61. Yin, Z., Haynie, J., Yang, X., Han, B., Kiatchoosakun, S., Restivo, J., Yuan, S., Prabhakar, N.R., Herrup, K., Conlon, R.A., et al. (2002). The essential role of Cited2, a negative regulator for HIF-1alpha, in heart development and neurulation. Proc. Natl. Acad. Sci. USA *99*, 10488–10493. https://doi.org/10.1073/pnas.162371799.
62. Browaeys, R., Saelens, W., and Saeys, Y. (2020). NicheNet: modeling intercellular communication by linking ligands to target genes. Nat. Methods *17*, 159–162. https://doi.org/10.1038/s41592-019-0667-5.
63. Rose-John, S. (2018). Interleukin-6 Family Cytokines. Cold Spring Harb. Perspect. Biol. *10*, a028415. https://doi.org/10.1101/cshperspect.a028415.
64. Bruce, A.G., Linsley, P.S., and Rose, T.M. (1992). Oncostatin M. Prog. Growth Factor Res. *4*, 157–170. https://doi.org/10.1016/0955-2235(92)90029-h.
65. Francis, A., Bosio, E., Stone, S.F., Fatovich, D.M., Arendts, G., MacDonald, S.P.J., Burrows, S., and Brown, S.G.A. (2019). Markers Involved in Innate Immunity and Neutrophil Activation are Elevated during Acute Human Anaphylaxis: Validation of a Microarray Study. J. Innate Immun. *11*, 63–73. https://doi.org/10.1159/000492301.
66. Berger, S.T., Ahmed, S., Muntel, J., Cuevas Polo, N., Bachur, R., Kentsis, A., Steen, J., and Steen, H. (2015). MStern Blotting-High Throughput Polyvinylidene Fluoride (PVDF) Membrane-Based Proteomic Sample Preparation for 96-Well Plates. Mol. Cell. Proteomics. *14*, 2814–2823. https://doi.org/10.1074/mcp.O115.049650.
67. Bennike, T.B., and Steen, H. (2017). High-Throughput Parallel Proteomic Sample Preparation Using 96-Well Polyvinylidene Fluoride (PVDF) Membranes and C18 Purification Plates. Methods Mol. Biol. *1619*, 395–402. https://doi.org/10.1007/978-1-4939-7057-5_27.
68. Leeman, H., Kaminska, E., Green, D., Bodman-Smith, M., Gravett, A., Bodman-Smith, K., Copier, J., Coulton, G., Fusi, A., and Dalgleish, A.G. (2019). Serum Apolipoprotein E and Other Inflammatory Markers Can Identify Non-Responding Patients to a Dendritic Cell Vaccine. Transl. Oncol. *12*, 397–403. https://doi.org/10.1016/j.tranon.2018.11.002.
69. Bennike, T.B., Bellin, M.D., Xuan, Y., Stensballe, A., Møller, F.T., Beilman, G.J., Levy, O., Cruz-Monserrate, Z., Andersen, V., Steen, J., et al. (2018). A Cost-Effective High-Throughput Plasma and Serum Proteomics Workflow Enables Mapping of the Molecular Impact of Total Pancreatectomy with Islet Autotransplantation. J. Proteome Res. *17*, 1983–1992. https://doi.org/10.1021/acs.jproteome.8b00111.
70. Boada, P., Fatou, B., Belperron, A.A., Sigdel, T.K., Smolen, K.K., Wurie, Z., Levy, O., Ronca, S.E., Murray, K.O., Liberto, J., et al. (2022). Longitudinal serum proteomics analyses identify unique and overlapping host response pathways in Lyme disease and West Nile virus infection. Front. Immunol. *13*, 101284. https://doi.org/10.3389/fimmu.2022.1012824.
71. Gabay, C., and Kushner, I. (1999). Acute-phase proteins and other systemic responses to inflammation. N. Engl. J. Med. *340*, 448–454. https://doi.org/10.1056/NEJM199902113400607.
72. Cooper, E.H., Forbes, M.A., and Hambling, M.H. (1984). Serum beta 2-microglobulin and C reactive protein concentrations in viral infections. J. Clin. Pathol. *37*, 1140–1143. https://doi.org/10.1136/jcp.37.10.1140.
73. Wan, G., Zhaorigetu, S., Liu, Z., Kaini, R., Jiang, Z., and Hu, C.a.A. (2008). Apolipoprotein L1, a novel Bcl-2 homology domain 3-only lipid-binding protein, induces autophagic cell death. J. Biol. Chem. *283*, 21540–21549. https://doi.org/10.1074/jbc.M800214200.
74. Shive, C.L., Jiang, W., Anthony, D.D., and Lederman, M.M. (2015). Soluble CD14 is a nonspecific marker of monocyte activation. AIDS *29*, 1263–1265. https://doi.org/10.1097/QAD.0000000000000735.
75. Xu, G., Deng, F., Zuo, Q., Liu, L., Dou, K., Cheng, Z., Cao, W., Luo, C., Yu, C., Liu, S., and Zhu, Y. (2021). Virus-inducible IGFALS facilitates innate immune responses by mediating IRAK1 and TRAF6 activation. Cell. Mol. Immunol. *18*, 1587–1589. https://doi.org/10.1038/s41423-021-00649-0.
76. Kimura, Y., Nakai, Y., Shin, J., Hara, M., Takeda, Y., Kubo, S., Jeremiah, S.S., Ino, Y., Akiyama, T., Moriyama, K., et al. (2021). Identification of serum prognostic biomarkers of severe COVID-19 using a quantitative proteomic approach. Sci. Rep. *11*, 20638. https://doi.org/10.1038/s41598-021-98253-9.
77. Luan, H., Gu, W., Li, H., Wang, Z., Lu, L., Ke, M., Lu, J., Chen, W., Lan, Z., Xiao, Y., et al. (2021). Serum metabolomic and lipidomic profiling identifies diagnostic biomarkers for seropositive and seronegative rheumatoid arthritis patients. J. Transl. Med. *19*, 500. https://doi.org/10.1186/s12967-021-03169-7.

78. Argelaguet, R., Velten, B., Arnol, D., Dietrich, S., Zenz, T., Marioni, J.C., Buettner, F., Huber, W., and Stegle, O. (2018). Multi-Omics Factor Analysis-a framework for unsupervised integration of multi-omics data sets. Mol. Syst. Biol. *14*, e8124. https://doi.org/10.15252/msb.20178124.
79. Argelaguet, R., Arnol, D., Bredikhin, D., Deloro, Y., Velten, B., Marioni, J.C., and Stegle, O. (2020). MOFA+: a statistical framework for comprehensive integration of multi-modal single-cell data. Genome Biol. *21*, 111. https://doi.org/10.1186/s13059-020-02015-1.
80. Lemke, G., and Rothlin, C.V. (2008). Immunobiology of the TAM receptors. Nat. Rev. Immunol. *8*, 327–336.
81. Li, Y., Wang, Y., and Wu, P. (2019). 5′-Methylthioadenosine and Cancer: old molecules, new understanding. J. Cancer *10*, 927–936. https://doi.org/10.7150/jca.27160.
82. Nagan, N., and Zoeller, R.A. (2001). Plasmalogens: biosynthesis and functions. Prog. Lipid Res. *40*, 199–229. https://doi.org/10.1016/s0163-7827(01)00003-0.
83. Vishnu, V.V., Muralikrishna, B., Verma, A., Nayak, S.C., Sowpati, D.T., Radha, V., and Shekar, P.C. (2021). C3G Regulates STAT3, ERK, Adhesion Signaling, and Is Essential for Differentiation of Embryonic Stem Cells. Stem Cell Rev. Rep. *17*, 1465–1477. https://doi.org/10.1007/s12015-021-10136-8.
84. Fraisier, C., Camoin, L., Lim, S.M., Bakli, M., Belghazi, M., Fourquet, P., Granjeaud, S., Osterhaus, A.D.M.E., Koraka, P., Martina, B., and Almeras, L. (2013). Altered protein networks and cellular pathways in severe west nile disease in mice. PLoS One *8*, e68318. https://doi.org/10.1371/journal.pone.0068318.
85. Aalto-Setälä, K., Fisher, E.A., Chen, X., Chajek-Shaul, T., Hayek, T., Zechner, R., Walsh, A., Ramakrishnan, R., Ginsberg, H.N., and Breslow, J.L. (1992). Mechanism of hypertriglyceridemia in human apolipoprotein (apo) CIII transgenic mice. Diminished very low density lipoprotein fractional catabolic rate associated with increased apo CIII and reduced apo E on the particles. J. Clin. Invest. *90*, 1889–1900. https://doi.org/10.1172/JCI116066.
86. Shi, Y., and Holtzman, D.M. (2018). Interplay between innate immunity and Alzheimer disease: APOE and TREM2 in the spotlight. Nat. Rev. Immunol. *18*, 759–772. https://doi.org/10.1038/s41577-018-0051-1.
87. Schwab, M.A., Sauer, S.W., Okun, J.G., Nijtmans, L.G.J., Rodenburg, R.J.T., van den Heuvel, L.P., Dröse, S., Brandt, U., Hoffmann, G.F., Ter Laak, H., et al. (2006). Secondary mitochondrial dysfunction in propionic aciduria: a pathogenic role for endogenous mitochondrial toxins. Biochem. J. *398*, 107–112. https://doi.org/10.1042/BJ20060221.
88. Han, Y.M., Ramprasath, T., and Zou, M.H. (2020). beta-hydroxybutyrate and its metabolic effects on age-associated pathology. Exp. Mol. Med. *52*, 548–555. https://doi.org/10.1038/s12276-020-0415-z.
89. Tsioris, K., Gupta, N.T., Ogunniyi, A.O., Zimnisky, R.M., Qian, F., Yao, Y., Wang, X., Stern, J.N.H., Chari, R., Briggs, A.W., et al. (2015). Neutralizing antibodies against West Nile virus identified directly from human B cells by single-cell analysis and next generation sequencing. Integr. Biol. *7*, 1587–1597. https://doi.org/10.1039/C5IB00169B.
90. Kapellos, T.S., Bonaguro, L., Gemünd, I., Reusch, N., Saglam, A., Hinkley, E.R., and Schultze, J.L. (2019). Human Monocyte Subsets and Phenotypes in Major Chronic Inflammatory Diseases. Front. Immunol. *10*, 2035. https://doi.org/10.3389/fimmu.2019.02035.
91. Constant, O., Barthelemy, J., Nagy, A., Salinas, S., and Simonin, Y. (2022). West Nile Virus Neuroinfection in Humans: Peripheral Biomarkers of Neuroinflammation and Neuronal Damage. Viruses *14*. https://doi.org/10.3390/v14040756.
92. Boyer, S., Lee, H.-J., Steele, N., Zhang, L., Sajjakulnukit, P., Andren, A., Ward, M.H., Singh, R., Basrur, V., Zhang, Y., et al. (2022). Multiomic characterization of pancreatic cancer-associated macrophage polarization reveals deregulated metabolic programs driven by the GM-CSF–PI3K pathway. Elife *11*, e73796. https://doi.org/10.7554/eLife.73796.
93. Chou, C.H., Mohanty, S., Kang, H.A., Kong, L., Avila-Pacheco, J., Joshi, S.R., Ueda, I., Devine, L., Raddassi, K., Pierce, K., et al. (2022). Metabolomic and transcriptomic signatures of influenza vaccine response in healthy young and older adults. Aging Cell *21*, e13682. https://doi.org/10.1111/acel.13682.
94. Guo, C., Xie, S., Chi, Z., Zhang, J., Liu, Y., Zhang, L., Zheng, M., Zhang, X., Xia, D., Ke, Y., et al. (2016). Bile Acids Control Inflammation and Metabolic Disorder through Inhibition of NLRP3 Inflammasome. Immunity *45*, 944. https://doi.org/10.1016/j.immuni.2016.10.009.
95. Diamond, M.S., Shrestha, B., Marri, A., Mahan, D., and Engle, M. (2003). B cells and antibody play critical roles in the immediate defense of disseminated infection by West Nile encephalitis virus. J. Virol. *77*, 2578–2586.
96. Sajid, A., Matias, J., Arora, G., Kurokawa, C., DePonte, K., Tang, X., Lynn, G., Wu, M.J., Pal, U., Strank, N.O., et al. (2021). mRNA vaccination induces tick resistance and prevents transmission of the Lyme disease agent. Sci. Transl. Med. *13*, eabj9827. https://doi.org/10.1126/scitranslmed.abj9827.
97. Puerta-Guardo, H., Glasner, D.R., Espinosa, D.A., Biering, S.B., Patana, M., Ratnasiri, K., Wang, C., Beatty, P.R., and Harris, E. (2019). Flavivirus NS1 Triggers Tissue-Specific Vascular Endothelial Dysfunction Reflecting Disease Tropism. Cell Rep. *26*, 1598–1613.e8. https://doi.org/10.1016/j.celrep.2019.01.036.
98. Lanteri, M.C., Heitman, J.W., Owen, R.E., Busch, T., Gefter, N., Kiely, N., Kamel, H.T., Tobler, L.H., Busch, M.P., and Norris, P.J. (2008). Comprehensive analysis of west nile virus-specific T cell responses in humans. J. Infect. Dis. *197*, 1296–1306. https://doi.org/10.1086/586898.
99. Tian, Y., Seumois, G., De-Oliveira-Pinto, L.M., Mateus, J., Herrera-de la Mata, S., Kim, C., Hinz, D., Goonawardhana, N.D.S., de Silva, A.D., Premawansa, S., et al. (2019). Molecular Signatures of Dengue Virus-Specific IL-10/IFN-gamma Co-producing CD4 T Cells and Their Association with Dengue Disease. Cell Rep. *29*, 4482–4495.e4. https://doi.org/10.1016/j.celrep.2019.11.098.
100. Michlmayr, D., Pak, T.R., Rahman, A.H., Amir, E.A.D., Kim, E.Y., Kim-Schulze, S., Suprun, M., Stewart, M.G., Thomas, G.P., Balmaseda, A., et al. (2018). Comprehensive innate immune profiling of chikungunya virus infection in pediatric cases. Mol. Syst. Biol. *14*, e7862. https://doi.org/10.15252/msb.20177862.
101. Gould, C.V., Staples, J.E., Huang, C.Y.-H., Brault, A.C., and Nett, R.J. (2023). Combating West Nile Virus Disease — Time to Revisit Vaccination. N. Engl. J. Med. *388*, 1633–1636. https://doi.org/10.1056/NEJMp2301816.
102. Ulbert, S. (2019). West Nile virus vaccines - current situation and future directions. Hum. Vaccin. Immunother. *15*, 2337–2342. https://doi.org/10.1080/21645515.2019.1621149.
103. Noé, A., Cargill, T.N., Nielsen, C.M., Russell, A.J.C., and Barnes, E. (2020). The Application of Single-Cell RNA Sequencing in Vaccinology. J. Immunol. Res. *2020*, 8624963. https://doi.org/10.1155/2020/8624963.
104. Langfelder, P., and Horvath, S. (2008). WGCNA: an R package for weighted correlation network analysis. BMC Bioinf. *9*, 559. https://doi.org/10.1186/1471-2105-9-559.
105. Bates, D., Mächler, M., Bolker, B., and Walker, S. (2015). Fitting Linear Mixed-Effects Models Using lme4. J. Stat. Softw. *67*, 1–48. https://doi.org/10.18637/jss.v067.i01.
106. Xie, Z., Bailey, A., Kuleshov, M.V., Clarke, D.J.B., Evangelista, J.E., Jenkins, S.L., Lachmann, A., Wojciechowicz, M.L., Kropiwnicki, E., Jagodnik, K.M., et al. (2021). Gene Set Knowledge Discovery with Enrichr. Curr. Protoc. *1*, e90. https://doi.org/10.1002/cpz1.90.
107. Pang, Z., Chong, J., Zhou, G., de Lima Morais, D.A., Chang, L., Barrette, M., Gauthier, C., Jacques, P.É., Li, S., and Xia, J. (2021). MetaboAnalyst 5.0: narrowing the gap between raw spectra and functional insights. Nucleic Acids Res. *49*, W388–W396. https://doi.org/10.1093/nar/gkab382.
108. Wishart, D.S., Feunang, Y.D., Marcu, A., Guo, A.C., Liang, K., Vázquez-Fresno, R., Sajed, T., Johnson, D., Li, C., Karu, N., et al. (2018). HMDB 4.0: the human metabolome database for 2018. Nucleic Acids Res. *46*, D608–D617. https://doi.org/10.1093/nar/gkx1089.
109. Gorchakov, R., Gulas-Wroblewski, B.E., Ronca, S.E., Ruff, J.C., Nolan, M.S., Berry, R., Alvarado, R.E., Gunter, S.M., and Murray, K.O. (2019). Optimizing PCR Detection of West Nile Virus from Body Fluid Specimens to Delineate Natural History in an Infected Human Cohort. Int. J. Mol. Sci. *20*, 1934. https://doi.org/10.3390/ijms20081934.
110. Busch, M.P., Kleinman, S.H., Tobler, L.H., Kamel, H.T., Norris, P.J., Walsh, I., Matud, J.L., Prince, H.E., Lanciotti, R.S., Wright, D.J., et al. (2008). Virus and antibody dynamics in acute west nile virus infection. J. Infect. Dis. *198*, 984–993.
111. Yao, Y., Liu, R., Shin, M.S., Trentalange, M., Allore, H., Nassar, A., Kang, I., Pober, J.S., and Montgomery, R.R. (2014). CyTOF supports efficient detection of immune cell subsets from small samples. J. Immunol. Methods *415*, 1–5. https://doi.org/10.1016/j.jim.2014.10.010.
112. Kleinsteuber, K., Corleis, B., Rashidi, N., Nchinda, N., Lisanti, A., Cho, J.L., Medoff, B.D., Kwon, D., and Walker, B.D. (2016). Standardization and quality control for

high-dimensional mass cytometry studies of human samples. Cytometry. A. *89*, 903–913. https://doi.org/10.1002/cyto.a.22935.

113. Finck, R., Simonds, E.F., Jager, A., Krishnaswamy, S., Sachs, K., Fantl, W., Pe'er, D., Nolan, G.P., and Bendall, S.C. (2013). Normalization of mass cytometry data with bead standards. Cytometry. A. *83*, 483–494. https://doi.org/10.1002/cyto.a.22271.

114. Hughes, T.K., Wadsworth, M.H., 2nd, Gierahn, T.M., Do, T., Weiss, D., Andrade, P.R., Ma, F., de Andrade Silva, B.J., Shao, S., Tsoi, L.C., et al. (2020). Second-Strand Synthesis-Based Massively Parallel scRNA-Seq Reveals Cellular States and Molecular Features of Human Inflammatory Skin Pathologies. Immunity *53*, 878–894.e7. https://doi.org/10.1016/j.immuni.2020.09.015.

115. Dobin, A., Davis, C.A., Schlesinger, F., Drenkow, J., Zaleski, C., Jha, S., Batut, P., Chaisson, M., and Gingeras, T.R. (2013). STAR: ultrafast universal RNA-seq aligner. Bioinformatics *29*, 15–21. https://doi.org/10.1093/bioinformatics/bts635.

116. Macosko, E.Z., Basu, A., Satija, R., Nemesh, J., Shekhar, K., Goldman, M., Tirosh, I., Bialas, A.R., Kamitaki, N., Martersteck, E.M., et al. (2015). Highly Parallel Genome-wide Expression Profiling of Individual Cells Using Nanoliter Droplets. Cell *161*, 1202–1214. https://doi.org/10.1016/j.cell.2015.05.002.

117. Becht, E., McInnes, L., Healy, J., Dutertre, C.A., Kwok, I.W.H., Ng, L.G., Ginhoux, F., and Newell, E.W. (2018). Dimensionality reduction for visualizing single-cell data using UMAP. Nat. Biotechnol. *37*, 38–44. https://doi.org/10.1038/nbt.4314.

118. Kazer, S.W., Aicher, T.P., Muema, D.M., Carroll, S.L., Ordovas-Montanes, J., Miao, V.N., Tu, A.A., Ziegler, C.G.K., Nyquist, S.K., Wong, E.B., et al. (2020). Integrated single-cell analysis of multicellular immune dynamics during hyperacute HIV-1 infection. Nat. Med. *26*, 511–518. https://doi.org/10.1038/s41591-020-0799-2.

119. Lloyd-Price, J., Arze, C., Ananthakrishnan, A.N., Schirmer, M., Avila-Pacheco, J., Poon, T.W., Andrews, E., Ajami, N.J., Bonham, K.S., Brislawn, C.J., et al. (2019). Multi-omics of the gut microbial ecosystem in inflammatory bowel diseases. Nature *569*, 655–662. https://doi.org/10.1038/s41586-019-1237-9.

120. Storey, J.D., and Tibshirani, R. (2003). Statistical significance for genomewide studies. Proc. Natl. Acad. Sci. USA *100*, 9440–9445. https://doi.org/10.1073/pnas.1530509100.

STAR★METHODS

KEY RESOURCES TABLE

REAGENT or RESOURCE	SOURCE	IDENTIFIER
Antibodies		
Metal-conjugated or carrier-free antibodies	Fluidigm/BioLegend	See Table S1.
Biological samples		
Blood draws from WNV infected participants	Baylor College of Medicine	N/A
Veri-Cells™ Lyophilized Human Control Cells	BioLegend	Cat#427201
Chemicals, peptides, and recombinant proteins		
EQ Four Element Calibration Beads	Fluidigm	Product Number 201078
Critical commercial assays		
MaxPar X8 labeling kits	Fluidigm	https://store.standardbio.com/Cytometry/ConsumablesandReagentsCytometry/MaxparAntibodyLabelingKits
Nextera XT DNA Library Preparation Kit	Illumina	#FC-131
Deposited data		
The de-identified patient data of CyTOF, Seq-Well, proteomics, and metabolomics (Year 1)	This paper	ImmPort: SDY1396; https://www.immport.org/shared/study/SDY1396
The de-identified patient data of CyTOF, Seq-Well, proteomics, and metabolomics (Year 2)	This paper	ImmPort: SDY1397; https://www.immport.org/shared/study/SDY1397
Demo data	This paper	https://bitbucket.org/kleinstein/projects/src/master/LeeZhaoFleming2023/
Software and algorithms		
CyTOF® Software v7.0	Standard BioTools	https://go.fluidigm.com/cytofsw/v7
Cytobank	Cytobank, Inc.	https://premium.cytobank.org/
Prism	GraphPad Software	https://www.graphpad.com
MATLAB 2021a	MathWorks	https://www.mathworks.com/products/matlab.html
Drop-seq pipeline	Broad Institute of MIT and Harvard	https://github.com/broadinstitute/Drop-seq
R software environment v3.6.1, v4.0.3, v4.0.5, v4.1.3	The R Foundation	https://www.r-project.org
R package *Seurat v3.1.5 or v4.0.1*	Stuart et al.[50]	https://satijalab.org/seurat/
R package *WGCNA v1.71*	Langfelder and Horvath[104]	https://horvath.genetics.ucla.edu/html/CoexpressionNetwork/Rpackages/WGCNA/
R package *nichenetr v1.0.0*	Browaeys et al.[62]	https://github.com/saeyslab/nichenetr
R package *MOFA2 v1.1.7*	Argelaguet et al.[78,79]	https://www.bioconductor.org/packages/release/bioc/html/MOFA2.html
R package *lme4*	Bates et al.[105]	https://github.com/lme4/lme4/
Enrichr	Xie et al.[106]	https://maayanlab.cloud/Enrichr/
MetaboAnalyst version 5.0	Pang et al.[107]	https://www.metaboanalyst.ca
Skyline software v20.2.1	MacCoss Lab	https://skyline.ms/project/home/software/Skyline/begin.view
TraceFinder version 3.3	Thermo Fisher Scientific	https://www.thermofisher.com/order/catalog/product/OPTON-31001

(*Continued on next page*)

Continued

REAGENT or RESOURCE	SOURCE	IDENTIFIER
Progenesis QI	Nonlinear Dynamics	https://www.nonlinear.com/progenesis/qi/
Analysis codes	This paper	https://bitbucket.org/kleinstein/projects/src/master/LeeZhaoFleming2023/
Other		
The Human Metabolome Database (HMDB)	Wishart et al.[108]	https://hmdb.ca

RESOURCE AVAILABILITY

Lead contact

Further information and requests for resources and reagents should be directed to and will be fulfilled by the lead contact, Ruth R. Montgomery (ruth.montgomery@yale.edu).

Materials availability

This study did not generate new unique reagents.

Data and code availability

- The de-identified patient data of CyTOF, Seq-Well, proteomics, and metabolomics supporting this study have been deposited at ImmPort (http://www.immport.org) and are publicly available as of the date of publication. Accession numbers are listed in the key resources table.
- All original code is available in this paper's supplemental information and also at this Bitbucket repository, https://bitbucket.org/kleinstein/projects/src/master/LeeZhaoFleming2023/.
- Any additional information required to reanalyze the data reported in this paper is available from the lead contact upon request.

EXPERIMENTAL MODEL AND STUDY PARTICIPANT DETAILS

Human study participants and ethics statement

This study was conducted in accordance with guidelines approved by the Human Investigations Committees of Baylor College of Medicine and Yale School of Medicine. A total of 11 participants were untreated and enrolled and samples collected with written informed consent approved annually by each institution. Demographics of study participants are shown in Table 1. All eligible patients infected with WNV during the enrollment period (n = 7) were recruited at Baylor College of Medicine within seven days of symptomatic onset of mild disease (fever only, WNF) or severe disease (invasive neurological illness such as encephalitis or meningitis, WNE) as defined by Center for Disease Control (CDC)-defined clinical criteria of neurologic involvement with infection confirmed by RT-PCR.[109] All eligible viremic asymptomatic donors during the enrollment period (n = 4) were identified at Gulf Coast Regional Blood Center donation sites (Houston, TX) through routine screening of blood by rapid nucleic acid test. As the threshold of WNV viremia detectable by the screening test indicates viral exposure occurred within 7 days[110] and asymptomatic participants (WNA) were enrolled 2–4 days following screening, duration of infection was comparable in both groups of participants. All participants regardless of symptoms showed antibody recognition of WNV envelope protein by immunoblot[33] to support comparison of immune responses directly. Asymptomatic donors had no acute illness and took no antibiotics or nonsteroidal anti-inflammatory drugs at the time of sampling. All enrolled participants were Caucasian. Other information such as ancestry and socioeconomic status was not available. Medical history was obtained at the time of enrollment. As this study specifically focuses on molecular characterization of symptomatic and asymptomatic infection responses, we did not include healthy uninfected individuals as their anti-WNV immune efficiency is undefined prior to infection. Due to the small cohort size, analysis of the influence or association of demographic factors was not performed, which limits this study's generalizability.

METHOD DETAILS

Sample collection and cell isolation

Blood samples were collected from WNV infected participants over a total period of 19 months taking advatgae of stable characteristics in individuals[34–36] with collection from each individual at enrollment (T1) and at 3-month (T2) and 1-year (T3) convalescent time points when participants had resolved their illnesses. Blood draws at Baylor College of Medicine were collected in BD Vacutainer tubes, sodium heparin tubes, or BD Vacutainer CPT Mononuclear Cell Preparation Tubes with Sodium Citrate as an anti-coagulant (BD Biosciences, #362761). Whole blood without anti-coagulant was collected for preparation of serum that was stored at −80°C until assay. Whole blood samples from sodium heparin tubes were processed in SMART tubes containing Proteomic Stabilizer PROT1 fixation buffer (SMART Tube, Inc., Las Vegas, NV), frozen on site according to the manufacturer's instructions, and shipped frozen. Blood samples in CPT tubes were processed within 2 h of collection according to the manufacturer's instructions and shipped overnight for processing the next day.[28] Fresh peripheral blood

mononuclear cells (PBMCs) were collected from CPT tubes, washed twice with 90% RPMI +10% FBS, and processed fresh for transcriptomics or cryopreserved in 10% DMSO, 90% FBS in liquid nitrogen at a concentration of 5 x 10^6cells/mL.

Cell labeling and mass cytometry acquisition

Cryopreserved whole blood samples were harvested from SMART tubes according to the manufacturer's instructions for mass cytometry (CyTOF). Samples were labeled with a uniform antibody cocktail as described previously.[39,111] Metal-conjugated antibodies (Table S1) for labeling cells were purchased from Fluidigm (Fluidigm Inc, South San Francisco, CA), or carrier-free antibodies were conjugated in house using MaxPar X8 labeling kits according to manufacturer's instructions (Fluidigm). Briefly, cells from SMART tubes were thawed in batches and washed with Maxpar Cell Staining Buffer (Fluidigm), incubated with surface labeling antibodies for 30 min on ice, permeabilized (BD FACS Perm II) for labeling with intracellular antibodies for 45 min on ice. Cells were suspended overnight in iridium interchelator (125 nM; Fluidigm) in 2% paraformaldehyde in PBS and washed 1X in PBS and 2X in H_2O immediately before acquisition. A spike-in reference sample of prelabeled Ta181-PBMC (BioLegend, Cat#427201, San Diego, CA) was added to each subject sample as a control to minimize the effects of batch variation.[112] Samples were run on Helios 2 CyTOF instrument at a flow rate of 30 μL/min and a minimum of 10,000 events was collected in the presence of EQ Calibration beads (Fluidigm) for normalization. An average of 17,870 ± 8,013 cells (mean ± s.d.) from each sample were acquired and analyzed by CyTOF.

CyTOF data processing and analysis

CyTOF FCS files were bead normalized using CyTOF Software v7.0.[113] Manual gating was performed on the Cytobank platform by exclusion of debris (Iridium^{low}, DNA^{low}), multi-cell events (Iridium^{hi}, DNA^{hi}), and doublets using the default data transformation of a hyperbolic arcsine.[39,111] Differences in frequencies of cell subsets between cohorts and time points were assessed by one-way ANOVA for multiple comparisons using Prism (GraphPad Software). Mean expression level of markers from spike-in reference cell data was assessed by PCA analysis and no significant difference was found between time points and severity groups thus no batch corrections were applied (Figure S1). For the functional status reflected by cell lineage-functional marker combinations, given the limited sample size, an exploratory statistical analysis was conducted using a permutation sampling approach. Mean channel intensity (arcsine) of functional markers was compared for the 580 cell type/marker combinations resulting in 274 combinations above a threshold of 20% expression for that marker. The fold change of mean responses for each cell type and marker was computed for symptomatic patients and asymptomatic cases. A distribution of permuted fold changes was determined for 1000 iterations of group assignment without replacement. Associated p values were computed from the rank of the observed fold change in the empirically constructed distribution using MATLAB 2021a.

Single cell transcriptional assays

PBMCs were washed twice in RPMI/10% FBS and residual red blood cells were lysed with 1x RBC Lysis Buffer (eBioscience, Invitrogen, #00433357) according to the manufacturer's instructions. Cells were processed for Seq-Well S^3 single-cell RNA-seq with second strand synthesis.[49,114] Cells were loaded on Seq-Well arrays at a density of 15,000 cells. Paired-end sequencing libraries were prepared from amplified cDNA with the Nextera XT DNA sample Prep Kit (Illumina, #FC-131) according to the manufacturer's instructions. Indexed cDNA libraries were pooled at equimolar ratios and sequenced on an Illumina NovaSeq 6000 system. Final libraries were sequenced with a 21-50-50 read structure. Libraries prepared from fresh or cryopreserved cell libraries were consistent and data from both methods are presented.

scRNA-seq raw data processing

BCL files were demultiplexed by nine base-pair assay barcodes (one 3′ and one 5′ barcode per assay) and converted to FASTQs using bcl2fastq. Paired end reads were aligned to the hg19 genome using STAR 2.7 alignment software[115] via the Broad Institute dropseq_workflow pipeline. To generate count matrices, reads were sorted on the cell level (where a 12 bp barcode corresponds to an individual cell/mRNA-capture bead) and then sorted on the transcript level (where an 8 bp barcode corresponds to a unique transcript), yielding gene-by-cell count matrices for each set of paired FASTQs. Low quality cells were filtered out if they had fewer than 500 total transcripts, fewer than 300 unique mapped genes, or more than 25% mitochondrial reads. The count matrices were log-normalized (with a scale-factor of 10,000) before further data-cleaning and downstream analysis.

scRNA-seq cell type identification

Cell types were identified by unsupervised clustering and differential expression analysis together with canonical lineage markers in an iterative manner using the Seurat R package.[50] First, 3,000 highly variable genes were selected from the merged dataset as detailed previously.[116] The distribution of expression for each gene was then centered around zero, using the Seurat package ScaleData function. These standardized expression values served as inputs for principal component analysis (PCA). The first n principal components (PCs) are selected to capture 75% of the variance and a k parameter for clustering was chosen as well ($\frac{1}{2} \times \sqrt{\text{total number of cells}}$). Using the top n = 13 PCs and the chosen k parameter (k = 130), a k-nearest neighbors' algorithm was applied using the Seurat package. A Shared Nearest Neighbor (SNN) graph was constructed, and clusters were established by the Seurat function, FindClusters (resolution parameter = 0.5). Clusters were visualized with the dimension reduction technique, Uniform Manifold Approximation and Projection (UMAP),[117] with a Wilcoxon rank-sum test to determine positive gene markers for each cluster compared to all other clusters (log-fold change >0.25 and an adjusted p value <0.05). Cell type

assignments for each cluster were assigned based on differentially expressed genes and the relative expression of 36 canonical lineage markers (Figure S4). Every cell type was re-clustered individually using the same method. At this re-clustered level, doublets (determined by co-expression of lineage markers) could be identified and filtered out and more refined cell types could be defined (e.g., identifying regulatory T cells within $CD4^+$ T cells). We first identified a total of 31 cell types (Figure S4) and then focused on 11 main PBMC cell types which largely correspond to our CyTOF data (Figure 3A): B cells, $CD14^+$ monocytes, $CD16^+$ monocytes, $CD4^+$ T cells, $CD8^+$ T cells, cDCs, pDCs, NK cells, plasma B cells, proliferating T cells, and Tregs.

Differential gene module discovery

We used the Weighted Gene Co-expression Network Analysis (WGCNA) framework[51,104] to discover *significant gene modules* for each cell type as detailed previously.[118] Gene co-expression was considered across all cells at all timepoints for each cell type and also within each time point for each cell type. As scRNA-seq data are typically very noisy with large numbers of dropout events, we did not assume that gene co-expression networks should follow a scale-free topology to determine the soft-power threshold. We instead used a fixed soft-power threshold of 5, which gives more consistency in terms of mean connectivity across different networks from our data. *Significant modules* were identified by comparing the observed module gene dissimilarity (from the topological overlap matrix) to 10,000 randomly generated gene modules using the Wilcoxon rank-sum test with FDR <0.05. Overall module expression was assessed by scores calculated by *AddModuleScore* in Seurat. We identified *differential modules*, among those *significant modules*, for 18 pairs of different disease severity states and time points (i.e., all 3 severity pairs x 3 timepoints and all 3 timepoint pairs x 3 severity states) by performing the Wilcoxon rank-sum test and the Kolmogorov-Smirnov (K-S) test for differential distributions of module scores in each condition pair in question (restricted to conditions with at least 10 cells). In addition, we examined distributions of fold changes between all condition pairs for each module. p-values from the Wilcoxon and K-S tests were systematically varied from 0.001 to 0.1 (from 0.001 to 0.009 by 0.001 and from 0.01 to 0.1 by 0.01) without adjustment for multiple testing at this stage. This lenient filtering method favors identification of potentially relevant modules for subsequent analysis and biological interpretations. In this work, we deem *differential modules* to be those with the mean p value of the two tests <0.01 and the fold change of median module scores >1.3 in any of the 18 condition pairs (Tables S2 and S3). Genes in each differential module were ranked by Pearson correlation coefficients between gene expression values and module scores. For functional gene set enrichment analysis of modules, we used *Enrichr*.[106]

Intercellular communication predictions

To identify upstream ligands that affect expression patterns of the WGCNA-based differential gene modules above, we employed the NicheNet method that integrates prior knowledge of ligand-receptor interactions, signaling networks, and gene regulatory networks compiled from public data sources and validated using more than 100 microarray studies.[62] We considered the 11 cell types for both receiver and sender cells. Each differential gene module was considered as a gene group of interest in the receiver cells, i.e., a group of target genes for ligands in the sender cells for each cell type. NicheNet identifies "active" ligands that significantly changes expression of module genes by calculating ligand activity scores for ligand-target pairs. We note that active ligands are considered to be ligand genes that are expressed in >10% of the sender cells in question. We analyzed the top 20 active ligands for each differential gene module for each cell type.

Proteomics

Samples were processed according to the MStern blotting protocol developed in the Steen lab.[67,69] In brief, 1 μL of serum (~50 μg of proteins) was mixed in 100 μL of urea buffer (8M urea in 50 mM ammonium bicarbonate) without depleting any high abundance proteins. Following reduction (50 mM DTT) and alkylation (250 mM iodoacetamide) of the cysteine residues, 10–15 μg of proteins were loaded onto a 96-well plate with an activated and primed hydrophobic polyvinylidene fluoride (PVDF) membrane at the bottom (Multiscreen HTS 0.45 μm Hydrophobic High Protein Binding Membrane 96-well Filtration plate (Product No. MSIPS4510; Millipore-Sigma).[67,69] Trypsinization of the proteins adsorbed to the membrane was achieved by incubation with the trypsin for 2h at 37°C. Resulting tryptic peptides were eluted off the membrane with 40% acetonitrile (ACN)/0.1% formic acid (FA). The resulting peptide mixtures were subsequently desalted using a 96-well MACROSPIN C18 plate (TARGA, The NestGroup Inc.). The equivalent of 1 μg of peptide was analyzed using a microLC system (Nexera Mikros, Shimadzu, Columbia, MD) equipped with SHIM-Pack MC-C18 column (5 cm length, 300 μm internal diameter, 1.9 μm particle size, Shimadzu) coupled online to an LCMS 8060 triple quadrupole mass spectrometer (Shimadzu) operated in targeted 'multi reaction monitoring' (MRM) mode using a 10.3 min gradient (5–40% buffer B: acetonitrile with 0.1% formic acid).

The final scheduled MRM method monitored 1,887 transition pairs associated with 629 unique tryptic peptides and 306 proteins (i.e., 1–3 peptides per protein; 3 transition pairs per peptide). A detailed list of transitions is given in Table S4. Using Skyline software (v20.2.1), the average peptide intensities were calculated for each protein, and the protein abundance in all samples were exported into a.csv format file for further analysis in Prism and/or R.

Metabolomics

Serum metabolomic profiles of participant samples were measured using a combination of four LC-MS methods that measure complementary metabolite classes, as previously described[93,119]: two methods that measure polar metabolites, a method that measures metabolites of intermediate polarity (e.g., fatty acids and bile acids), and a lipid profiling method. For the analysis queue in each method, participants were randomized and longitudinal samples from each participant were randomized and analyzed as a group. A pooled QC sample for the LC-MS

methods was created by combining aliquots from each sample. Additionally, pairs of pooled reference samples were inserted into the queue at intervals of approximately 20 samples for QC and data standardization. Samples were prepared for each method using extraction procedures that are matched for use with the chromatography conditions. Data was acquired using LC-MS systems consisting of Nexera X2 U-HPLC systems (Shimadzu Scientific Instruments; Marlborough, MA) coupled to Q Exactive/Exactive Plus orbitrap mass spectrometers (Thermo Fisher Scientific; Waltham, MA).

HILIC-pos (positive ion mode MS analyses of polar metabolites), HILIC-neg (negative ion mode MS analysis of polar metabolites), C18-neg (negative ion mode analysis of metabolites of intermediate polarity (e.g., bile acids and free fatty acids), and C8-pos (positive ion mode analysis of polar and nonpolar lipids) LC-MS methods were carried out as previously described.[93]

Metabolomics data processing

Raw data were processed using TraceFinder 3.3 (Thermo Fisher Scientific; Waltham, MA) and Progenesis QI (Nonlinear Dynamics; Newcastle upon Tyne, UK). Peak identification was conducted by matching measured retention times (RT) and mass to charge ratios (m/z) to mixtures of reference metabolites analyzed in each batch. We matched unknown features to an internal database of >2600 compounds that have been characterized using methods as previously described.[93,119] This library contains compounds that have been confirmed by matching their RT, m/z and MS/MS fragmentation patterns in multiple human biofluids using authentic reference standards. To annotate unknowns based on this library, we used in-house alignment scripts to adjust the RT and m/z and match study unknowns to the compound library. No MS/MS was generated for this study. Temporal drift was monitored and normalized with the intensities of features measured in one of the doubly injected QC pooled reference samples using a nearest neighbor approach, where sample intensities in each pool are used to scale their closest samples. To determine the analytical precision for each measured metabolite, we computed coefficients of variation (CV) for annotated and unknown features using the remaining QC pools not used for scaling temporal drifts. Average CV values per method for annotated compounds was 7–11%, which is within the historical analytical. Finally, principal component analyses were generated and scores plots used to identify potential outlying samples.

For computational and statistical analysis of metabolomics data, relative metabolite intensities were pre-processed, normalized, and log-transformed. Undetected metabolites were imputed with half of the minimum value of that metabolite. Metabolites were median normalized within samples, and intensities were scaled by multiplying by 10^6 and log transformed to stabilize variance. We used the R package *lme4* to fit a linear mixed-effects model with age, gender, symptoms, and time as fixed effects and participants as random effects.[105] One-way ANOVA was used to test full vs. reduced model based on F-test to evaluate p values and corrected using multiple comparisons[120] to calculate false discovery rate (FDR). Full model: ~ Time + Symptoms + Age + Gender + l(1|Subject). Reduced model in the longitudinal group was ~ Symptoms + Age + Gender + (1|Subject) and in the symptoms group was ~ Time + Age + Gender + (1|Subject). Differentially abundant metabolites (DAM) were defined by thresholds of p value <0.05 and $|FC| \geq 1.2$ and FDR) estimation was performed from a collection of p values. We used the human metabolome database (HMDB)[108] to classify metabolites into subclass or pathway.

Multi-omics data integration

Data from all the assay platforms were integrated using a joint dimension reduction with multi-omics factor analysis (MOFA2) to construct multi-omics modules.[78,79] MOFA factors were derived to explain variabilities across samples for CyTOF (34 cell type proportions), per-cell type functional marker expression levels (580 combinations), proteomics (265 proteins), metabolomics (578 metabolites), Seq-Well cell-type-specific average gene expression levels (7610) and average cell-type-specific module expression levels from Seq-Well (47). The omics data were aligned for the 28 available samples. Each factor was linked to features from multiple omics, which allowed us to interpret their biological functions using public resources for different omics: Enrichr 115 for transcriptomics and proteomics (using two databases of KEGG_2021_Human and WikiPathway_2021_Human) and MetaboAnalyst 120 for metabolomics (using Over Representation Analysis by the hypergeometric test with default parameters). We assessed 7 MOFA factors and tested whether their factor scores were associated with different time points or disease states across samples. We performed an Analysis of Variance (ANOVA) test, and compared variance explained for each factor using time points, disease groups, or both. We also considered a Wilcoxon rank-sum test comparing the paired changes from acute phase to month 3 for different disease groups. These changes are calculated using the paired observation for each participant, i.e., the change Δ_i for participant i is calculated as $\Delta_i = X_{i2} - X_{i1}$, where X_{i1} is the factor score at the acute phase and X_{i2} is the factor score at month 3 for this participant. We then tested whether the distribution of Δ_i is the same for the asymptomatic group and the symptomatic group. Investigation of Δ_i can reveal dynamics in immune profiles during early infections. In addition, when interpreting MOFA features, we focused on a set of top features that meet either of the following two criteria: (1) factor-feature Pearson correlation p value <0.01 and (2) MOFA absolute weights > Q3 + 1.5*IQR, where Q3 is the third quartile and IQR is the interquartile range. Adjusted p values remain significant after multiple testing correction.

QUANTIFICATION AND STATISTICAL ANALYSIS

Student's *t* test and the chi-squre test were used for differences in age and sex between cohorts, respectively (Table 1). Differences in cell-type frequencies, expression levels of proteins, abundance levels of metabolites, and MOFA factor scores between cohorts and time points were assessed by ANOVA with Tukey's multiple comparisons or FDR or Wilcoxon rank-sum tests (Figures 1, 4, 5, 6, and S1). Changes in mean channel intensities of CyTOF markers among cell types were tested by a generalized linear mixed model (Figures 2 and S3). A combination of Wilcoxon rank-sum tests and Kolmogorov-Smirnov tests was used for differential gene module analysis (Figure 3B). All statistical parameters are described in method details.